

Supporting Information for

Titanocene and Zirconocene Complexes with Diaminoacetylenes – Formation of Unusual Metallacycles and Fulvene Complexes

**Òscar Àrias,[†] Alex R. Petrov,[†] Thomas Bannenberg,[†] Kai Altenburger,[‡] Perdita Arndt,[‡] Peter G.
Jones,[†] Uwe Rosenthal,^{*‡} Matthias Tamm^{*†}**

[†]Institut für Anorganische und Analytische Chemie, Technische Universität Braunschweig, Hagenring
30, D-38106 Braunschweig, Germany

[‡]Leibniz-Institut für Katalyse e.V. an der Universität Rostock, Albert-Einstein-Str. 29a, D-18059
Rostock, Germany

Contents:

1. Experimental Procedures	S2
2. NMR studies	S3
3. Kinetic study	S18
4. Crystallographic data	S22
5. Computational details	S23
6. References	S27
7. Appendix	S28

1. Experimental Procedures

1.1. Up-scaled and modified synthesis of $[\text{Cp}_2\text{Ti}(\eta^2\text{-btmsa})]$ (2).¹

A 100 mL Schlenk-tube was charged with a suspension of $[\text{Cp}_2\text{TiCl}_2]$ (5.0 g, 20 mmol) and Mg turnings (500 mg, 21 mmol, 1.03 equiv) in THF (30 mL). Then btmsa (5 mL, 22 mmol) was added and the reaction was initiated by sonication for 5–10 min at ambient temperature with occasional manual swirling until the pale-red supernatant turned dark red-orange. The reaction mixture was vigorously stirred without sonication, whereupon a mild exothermic reaction with dissolution of the starting material takes place. The reaction mixture was stirred for ca. 1 h at same temperature (*ca.* 45–50 °C). During the course of the reaction, a green crystalline precipitate appears first and then slowly dissolves yielding a dark brown solution with small amount of unreacted Mg turnings. All volatiles were removed in high vacuum and the product was extracted with pentane (20 mL); the solids were washed with the same solvent (4×5 mL). Cooling the reaction mixture to –78 °C results in crystallization of a yellow solid that was collected by decantation and dried in high vacuum. Yield: 75% (5.25 g) of a gold, fairly air-sensitive crystalline solid that possesses very high solubility in common organic solvents. The ^1H and $^{13}\text{C}\{^1\text{H}\}$ NMR spectroscopic data are in accord with those reported in the literature.

1.2. Modified synthesis of dichloride bis(η^5 -pentamethylcyclopentadienyl) zirconium(IV), $[\text{Cp}^*_2\text{ZrCl}_2]$.²

In a 250 mL-Schlenk flask was mixed ZrCl_4 (2.80 g, 12 mmol), Cp^*Na (4.22 g, 26.6 mmol, 1.11 equiv) and toluene (125 mL), and the heterogeneous mixture was refluxed for 3 h (120 °C). During this time, the solution turned dark brown, ZrCl_4 was completely dissolved and a very fine white precipitate was observed (NaCl). The mixture was filtered through a Celite[®]-pad (slow filtration) leaving a dark residue and a brown solution. The frit was washed with toluene (10 mL + 2×5 mL) and the solvent was removed, leaving an orange solid. The solid was washed with diethyl ether (50 mL), stirring the mixture for 2 h. The yellow suspension containing a fine white solid was filtered through a frit (no. 4) and the isolated pale yellow solid was dried in high vacuum and stored in a glove-box. Yield: 58%. ^1H NMR (300.1 MHz, CDCl_3): 1.99 ppm. $^{13}\text{C}\{^1\text{H}\}$ NMR (75.5 MHz, CDCl_3): 12.2 (C_5Me_5), 123.5 (C_5Me_5) ppm.

2. NMR studies

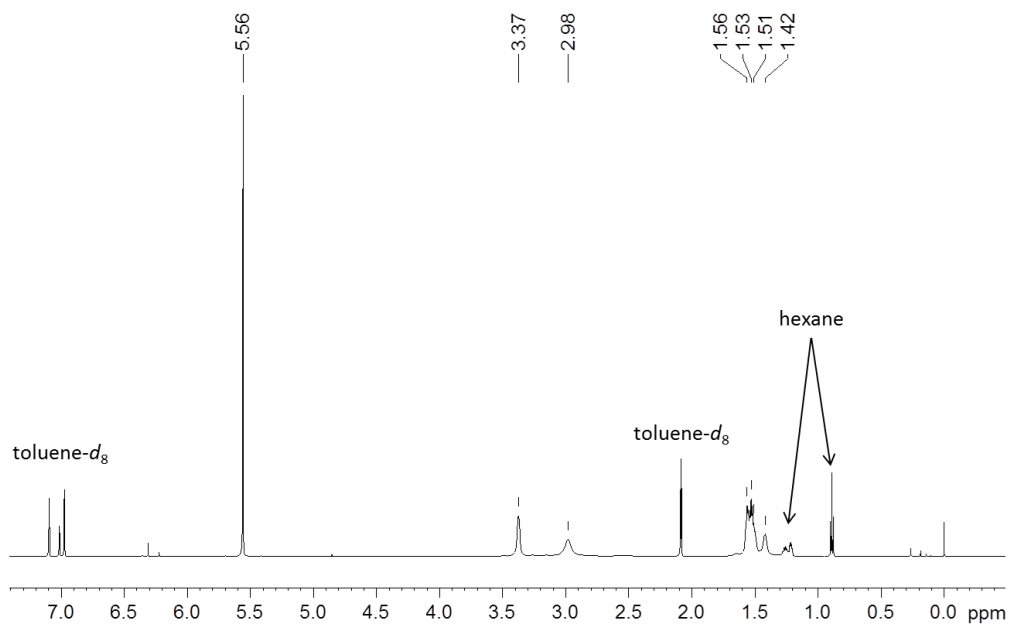
2.1. General considerations

NMR spectra were recorded on a Bruker DPX-200, Bruker AV II-300, Bruker AV II-400, Bruker DRX-400, and Bruker AV II-600 devices. The chemical shifts (δ) are expressed in ppm and are given relative to internal TMS ($\delta = 0.00$ ppm), to residual solvent ^1H signals (toluene- d_7 , $\delta_{\text{H}} = 2.08$ ppm; tetrahydrofuran- d_7 , $\delta_{\text{H}} = 3.58$ ppm; C_6HD_5 , $\delta_{\text{H}} = 7.16$ ppm) or to the ^{13}C resonance of the solvents (toluene- d_8 , $\delta_{\text{C}} = 20.43$ ppm; tetrahydrofuran- d_8 , $\delta_{\text{C}} = 67.21$ ppm; C_6D_6 , $\delta_{\text{C}} = 128.06$ ppm). The number of protons attached to each carbon was determined by ^{13}C -DEPT135 experiments. If required, signal assignment was achieved by two-dimensional H,H-COSY, H,H-NOESY, H,C-HSQC, and H,C-HMBC NMR experiments. The spectra were recorded using standard Bruker pulse programs; sweep widths, digital resolution, and pulse delays were optimized for the samples under investigation. Mixing times of 500, 1000 and 2000 ms were used for the H,H-NOESY experiments. For the low-temperature measurements, the temperature display of the spectrometer was calibrated against the standard methanol sample (4% methanol in methanol- d_4), whereas for the high-temperature measurements, it was calibrated against the standard glycol sample (80% glycol in DMSO- d_6).

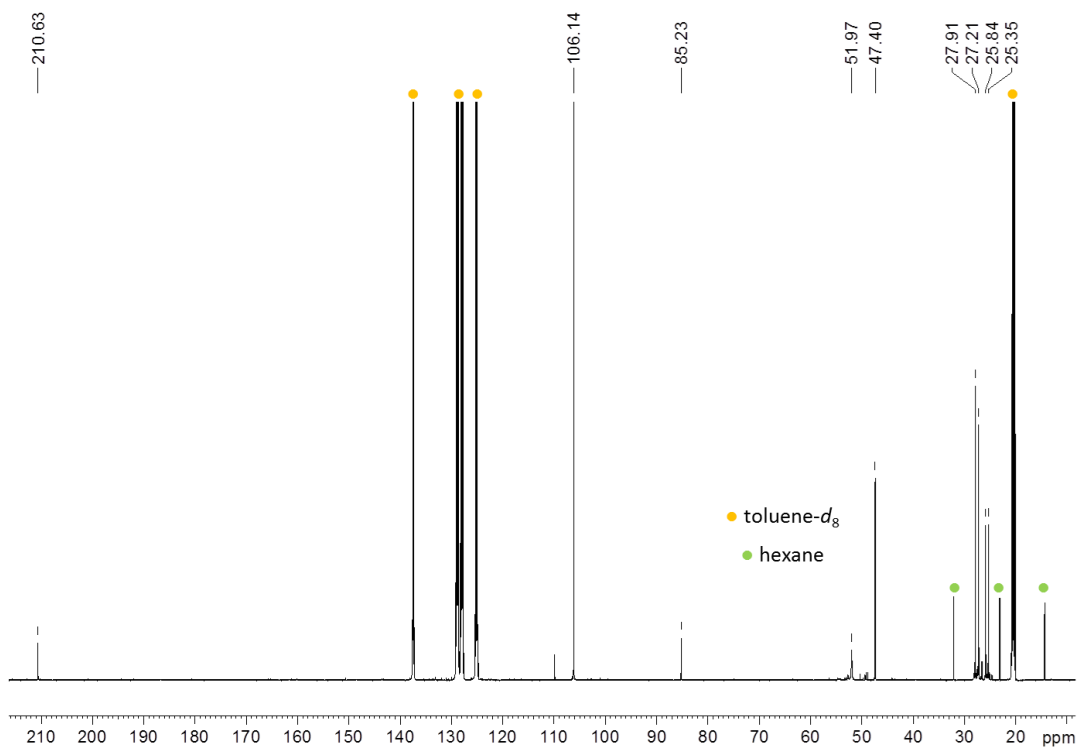
2.2. NMR spectra of all compounds

$[Cp_2Ti(C_4pip_4)]$ (3)

1H NMR (toluene- d_8 , 600.1 MHz, 295 K)

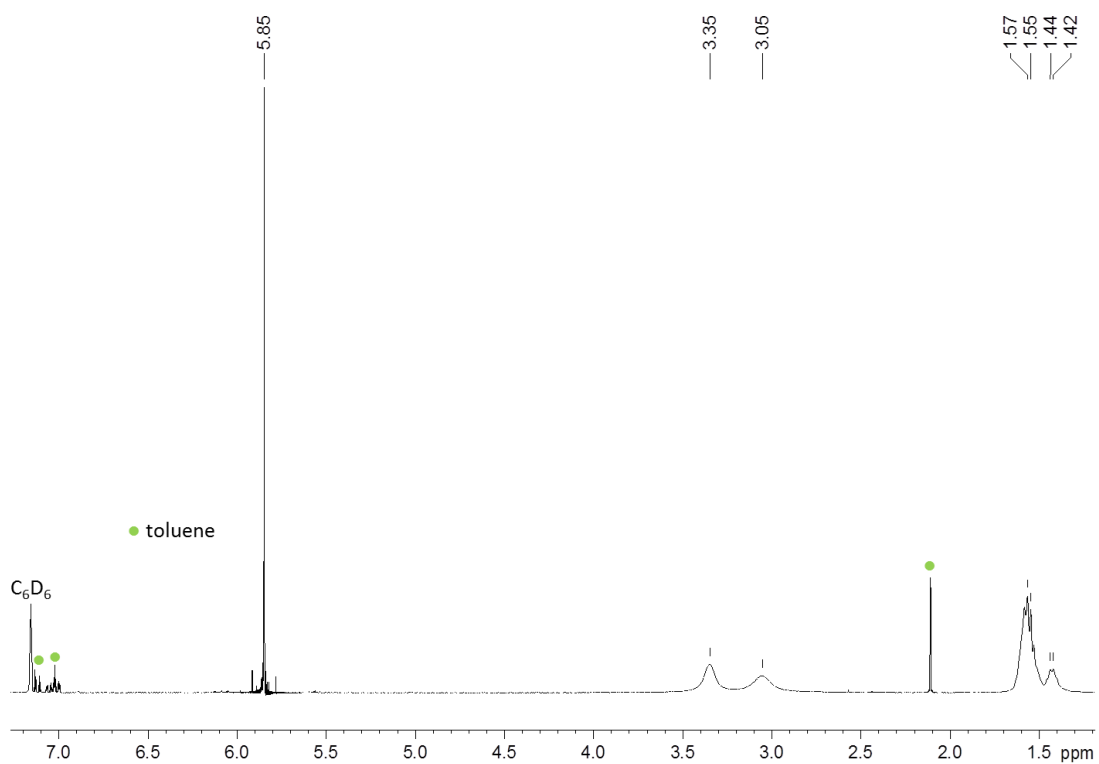


$^{13}C\{^1H\}$ NMR (toluene- d_8 , 150.9 MHz, 295 K)

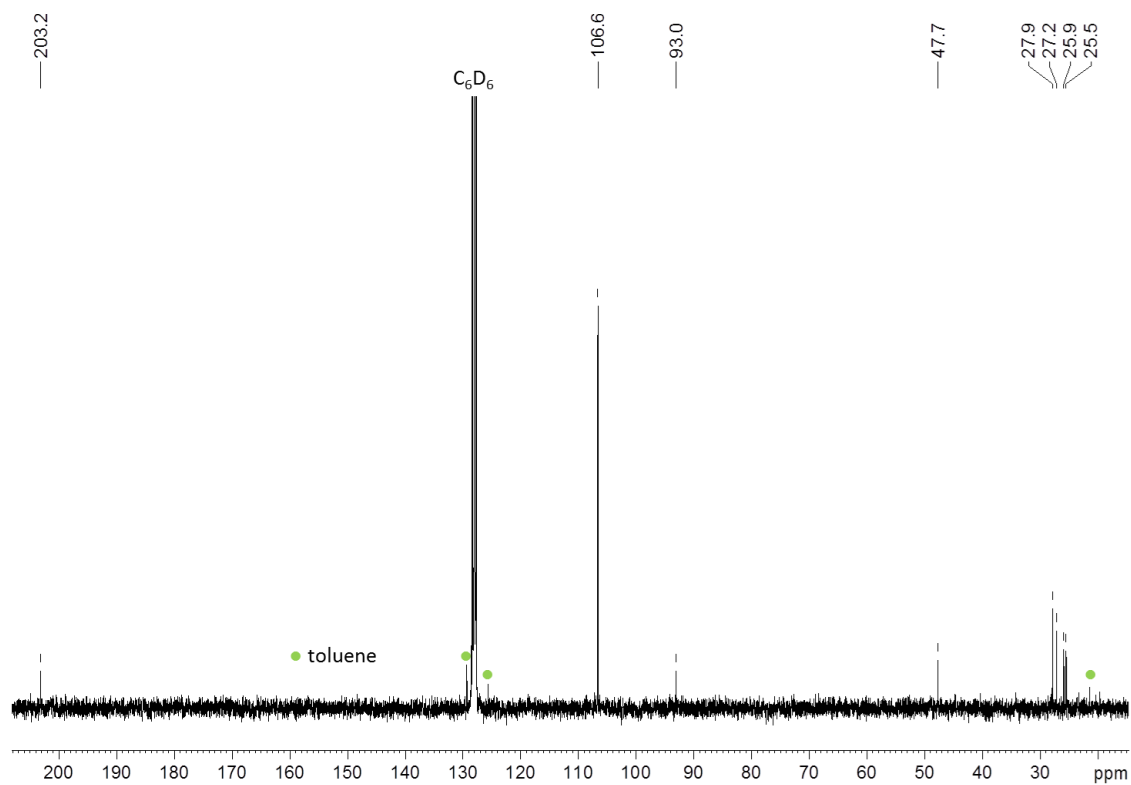


$[Cp_2Zr(C_4pip_4)]$ (5)

1H NMR (C_6D_6 , 300.1 MHz, 300 K)

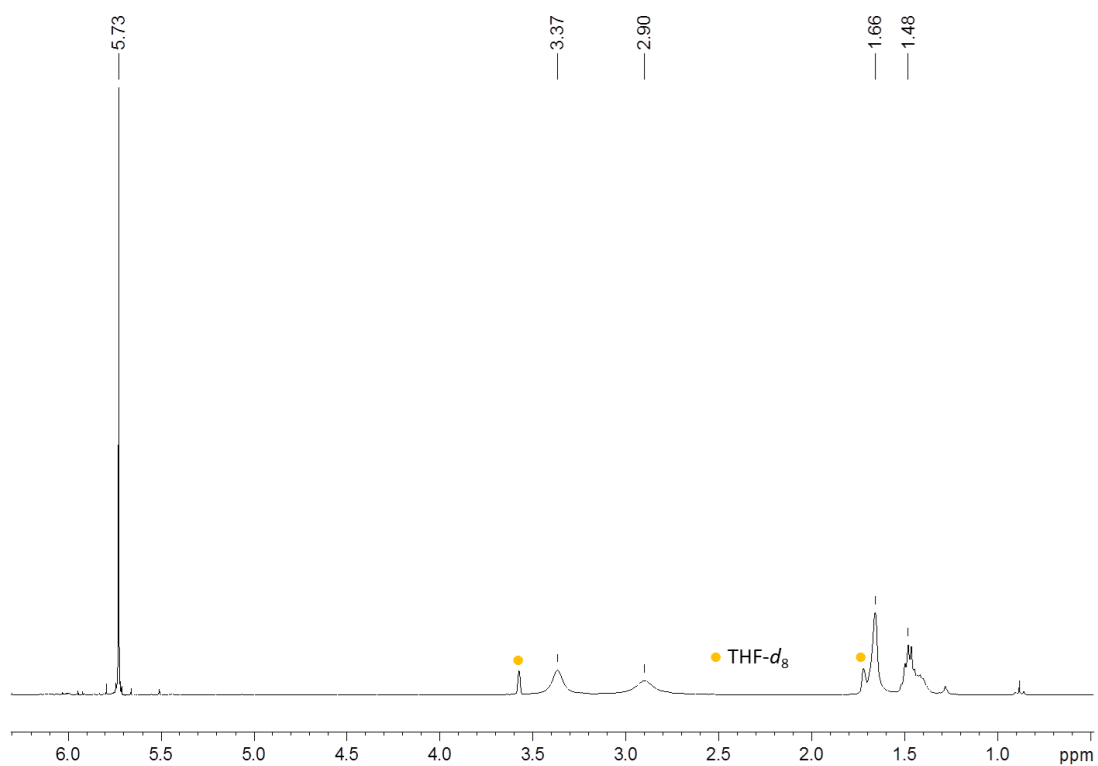


$^{13}C\{^1H\}$ NMR (C_6D_6 , 75.5 MHz, 300 K)

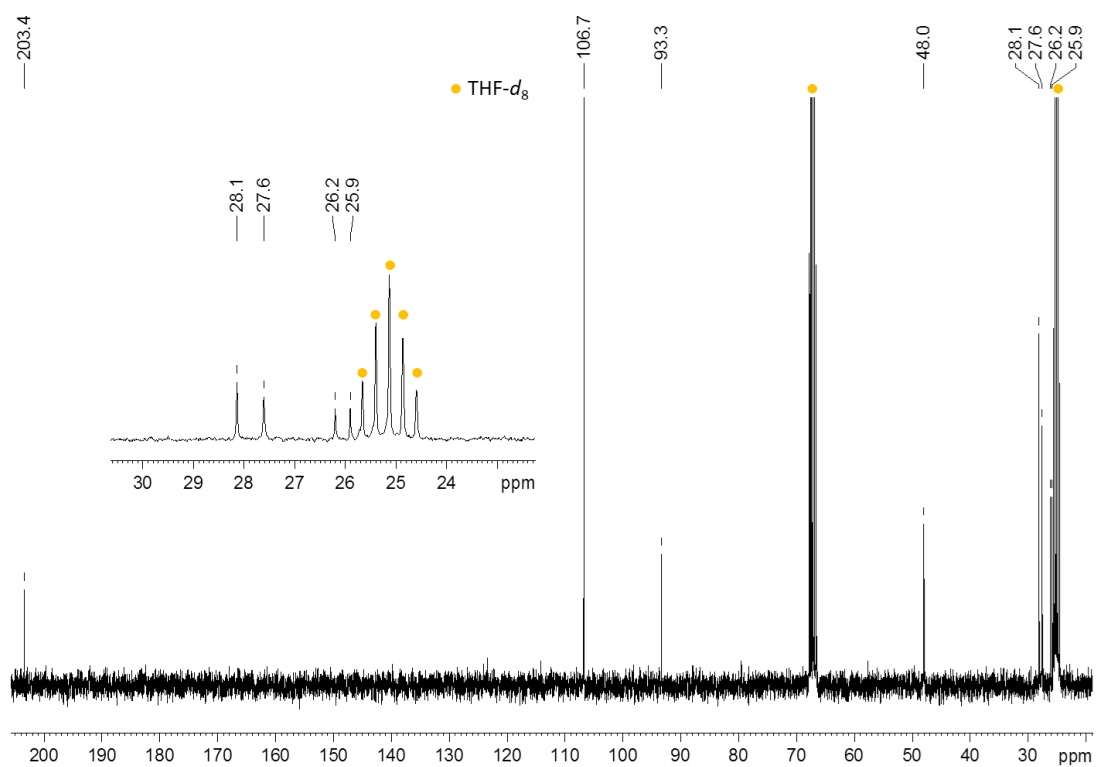




1H NMR (THF- d_8 , 300.1 MHz, 299 K)

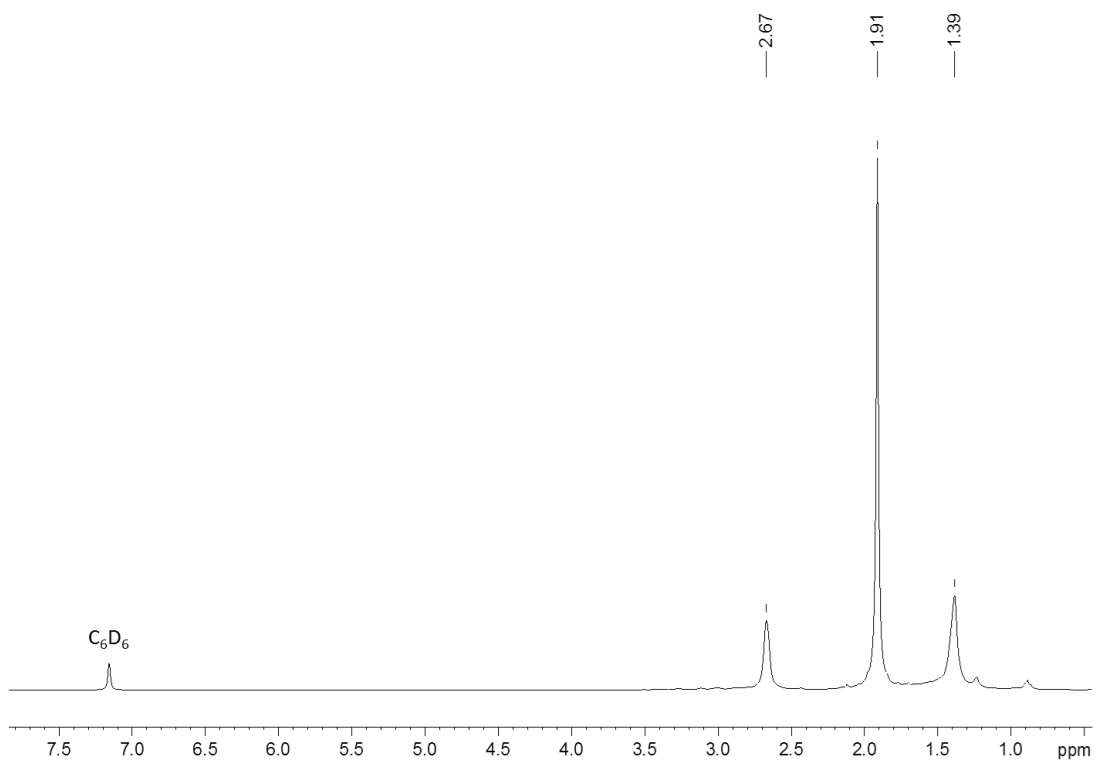


$^{13}C\{^1H\}$ NMR (THF- d_8 , 75.5 MHz, 300 K)

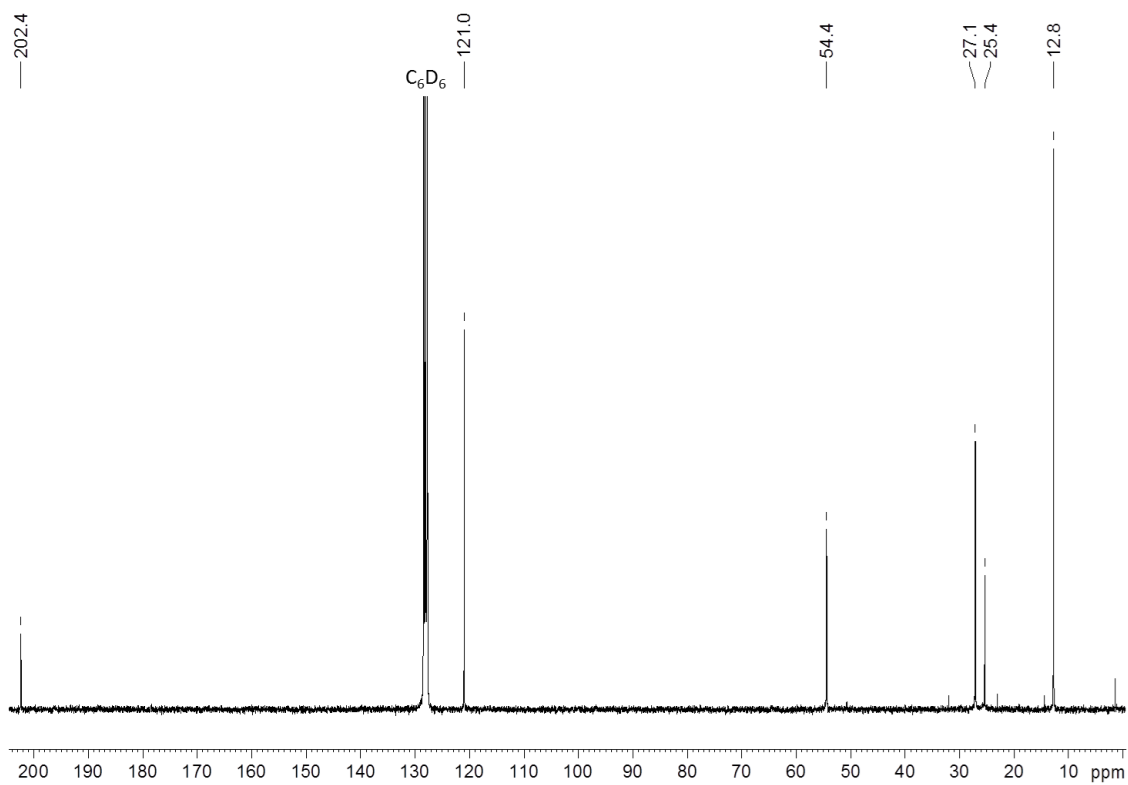


$[Cp^*_2Ti(C_2pip_2)]$ (7)

1H NMR (C_6D_6 , 300.1 MHz, 300 K)

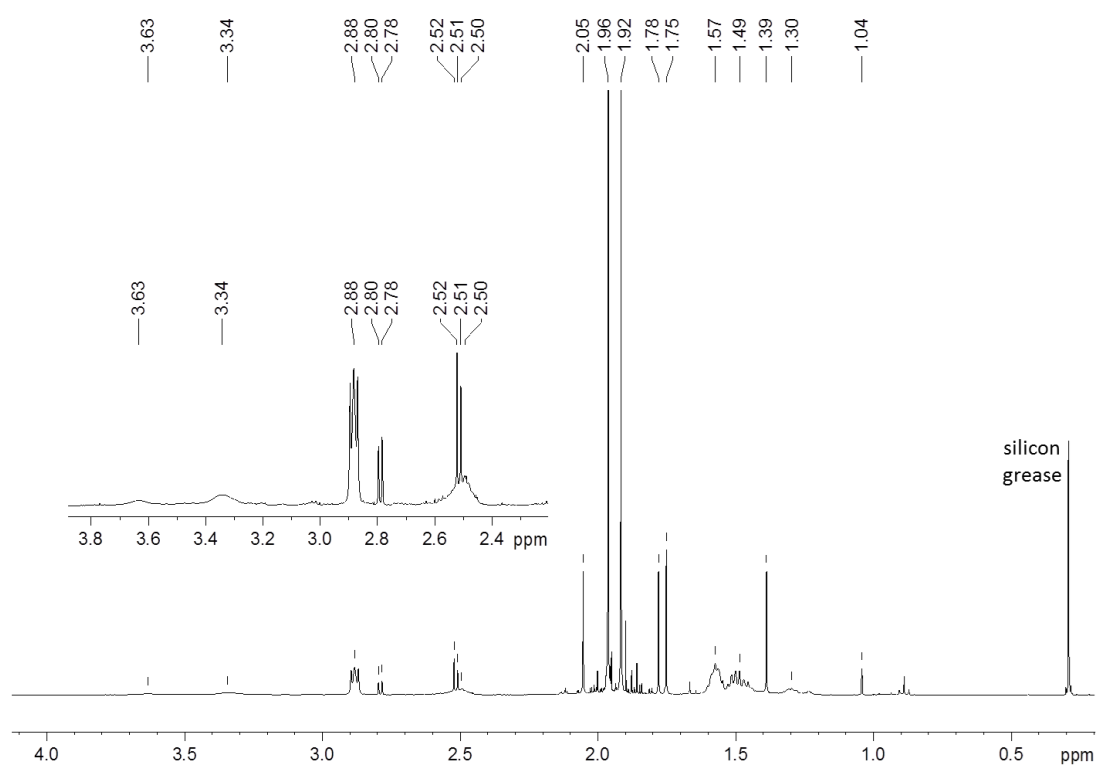


$^{13}C\{^1H\}$ NMR (C_6D_6 , 75.5 MHz, 300 K)

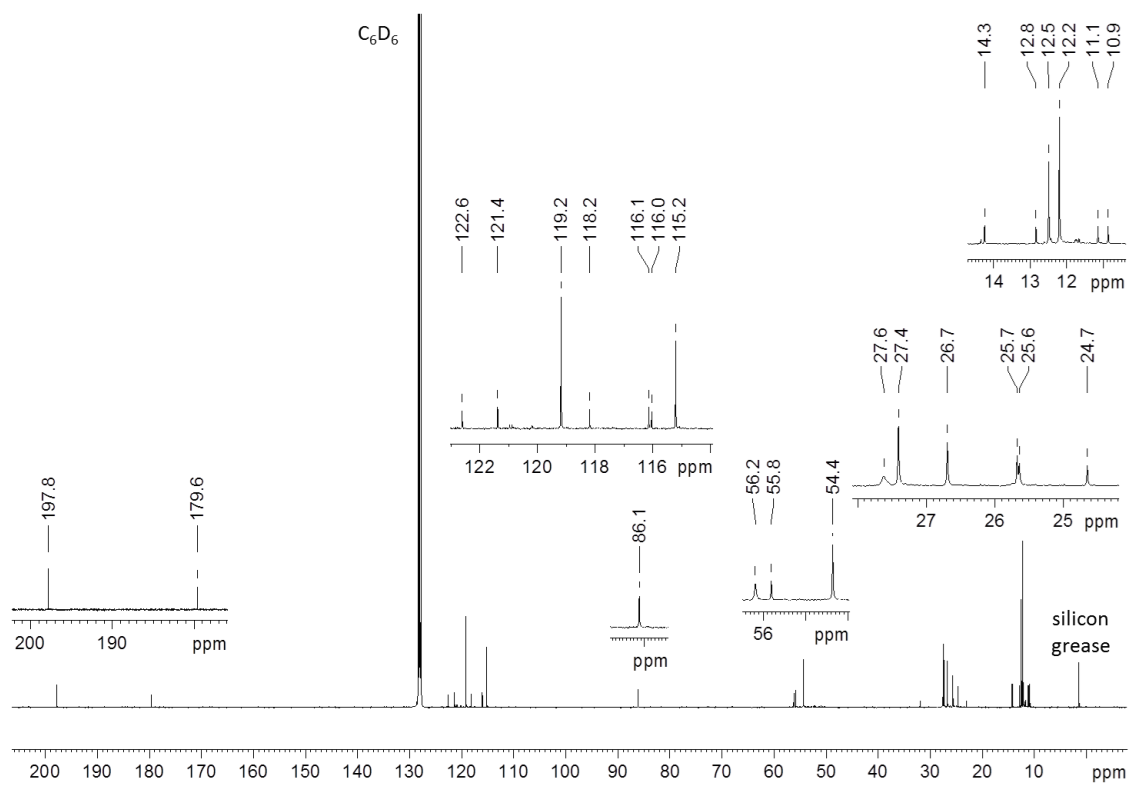




1H NMR (C_6D_6 , 400.4 MHz, 297 K)

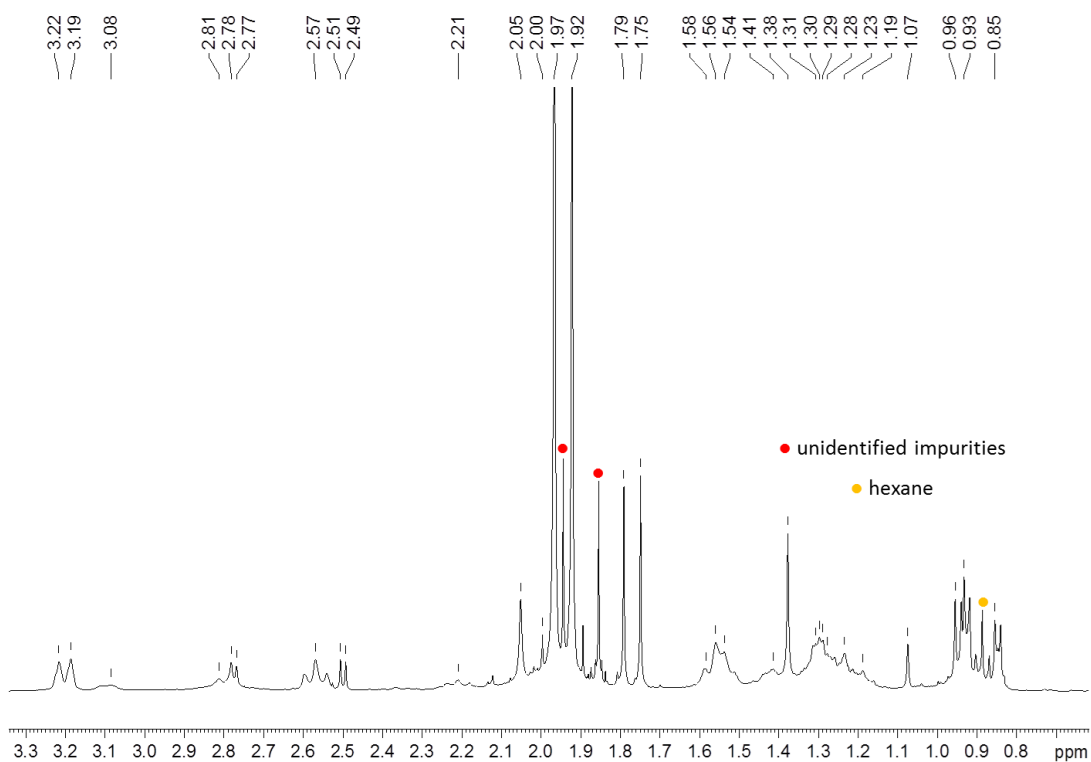


$^{13}C\{^1H\}$ NMR (C_6D_6 , 100.7 MHz, 299 K)

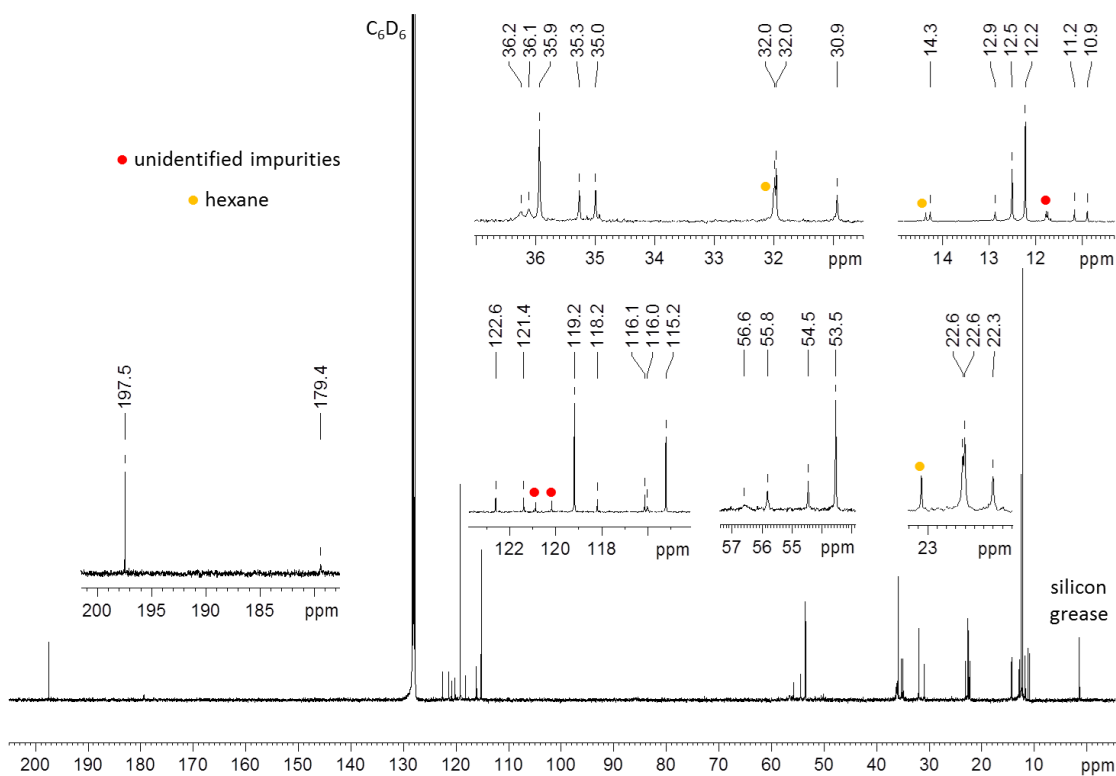




1H NMR (C_6D_6 , 399.9 MHz, 297 K)

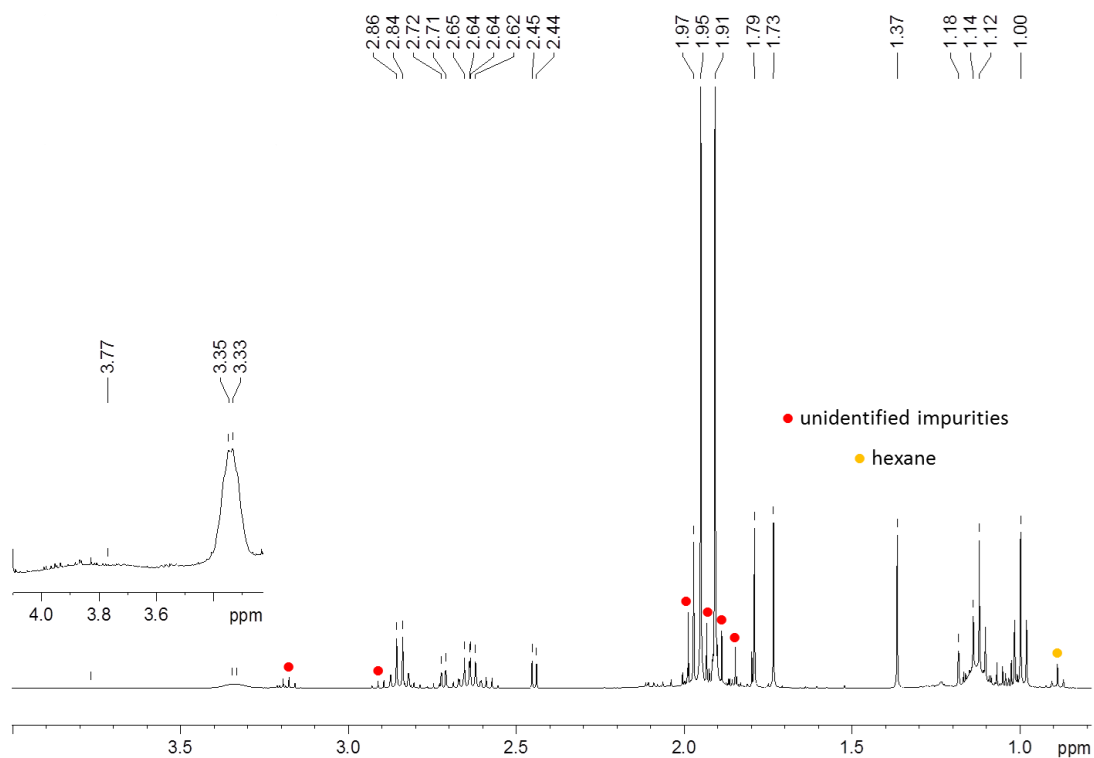


$^{13}C\{^1H\}$ NMR (C_6D_6 , 100.6 MHz, 299 K)

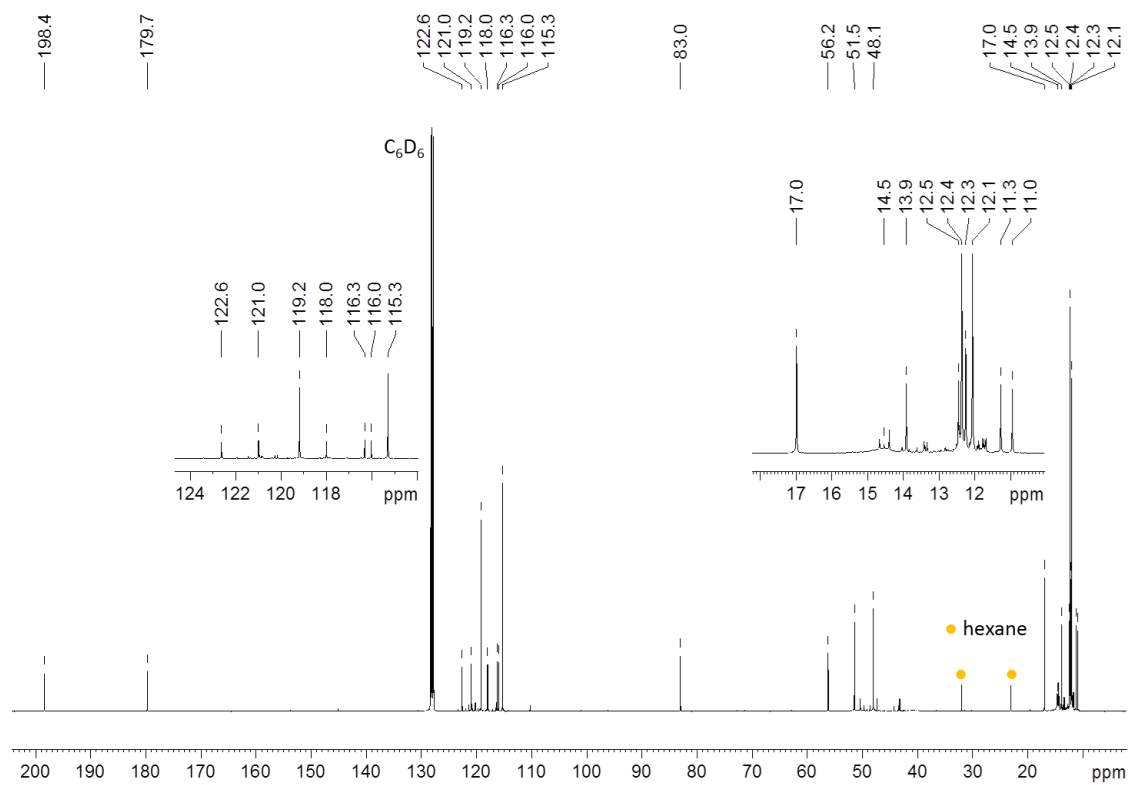




1H NMR (C_6D_6 , 400.4 MHz, 297 K)



$^{13}C\{^1H\}$ NMR (C_6D_6 , 100.7 MHz, 298 K)



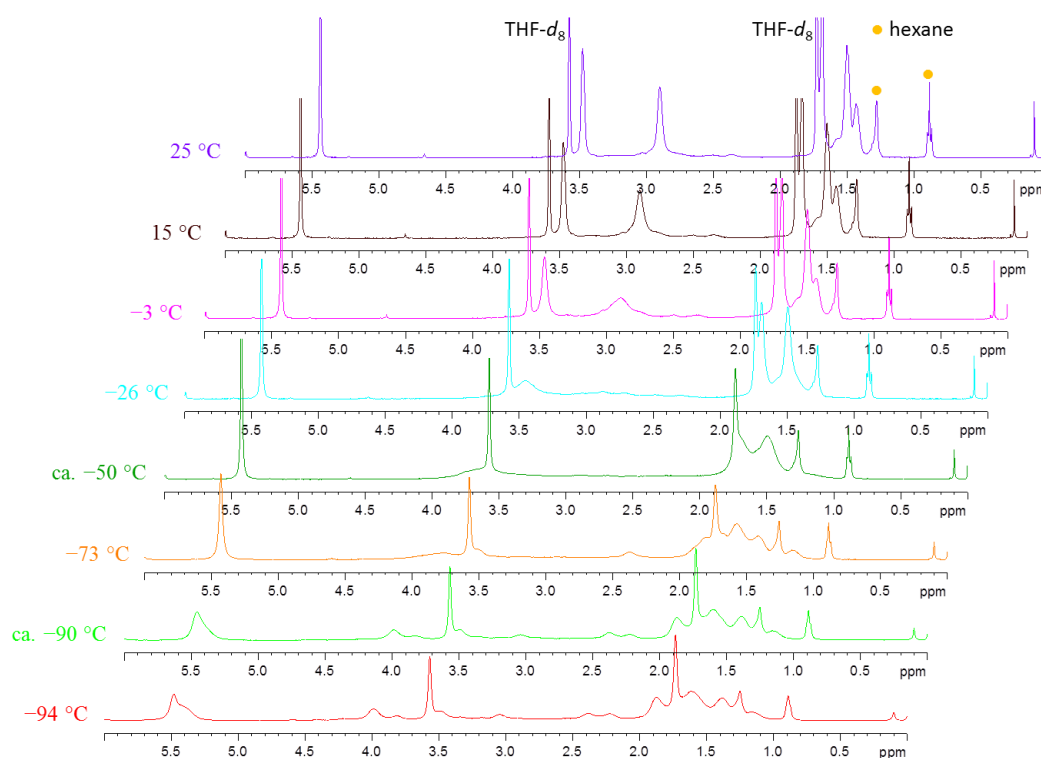
2.3. NMR investigations on complex [Cp₂Ti(C₄pip₄)] (**3**)

NMR data of **3** in C₆D₆. ¹H NMR (C₆D₆, 300.1 MHz, 300 K): δ = 1.41–1.57 (overlapped m, 16H, 3-, 4-, 5-CH₂), 3.02 (m, 4H, β-2,6-CH₂), 3.40 (s, 4H, α-2,6-CH₂), 5.64 (s, 5H, C₅H₅) ppm. ¹³C{¹H} NMR (C₆D₆, 75.5 MHz, 300 K): δ = 25.3 (α-4-CH₂), 25.8 (β-4-CH₂), 27.2 (α-3,5-CH₂), 27.9 (β-3,5-CH₂), 47.5 (β-2,6-CH₂), 52.0 (α-2,6-CH₂), 85.4 (β-C_q), 106.2 (C₅H₅), 211.2 (α-C_q) ppm.

Low temperature NMR spectroscopy in tetrahydrofuran-*d*₈ (399.9 MHz, 298–179 K)

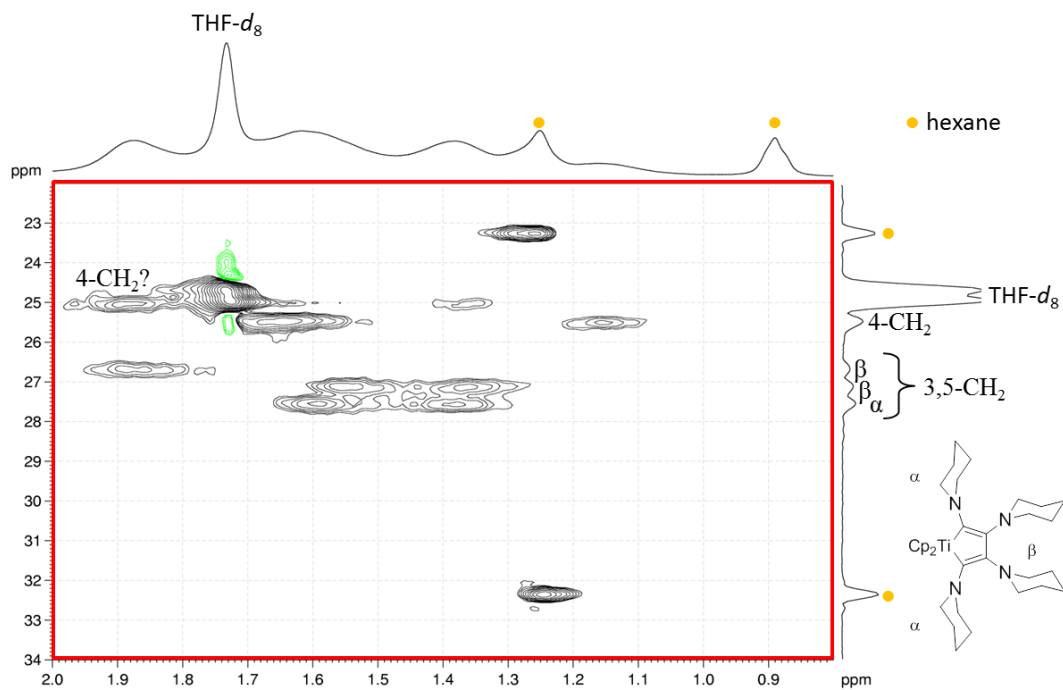
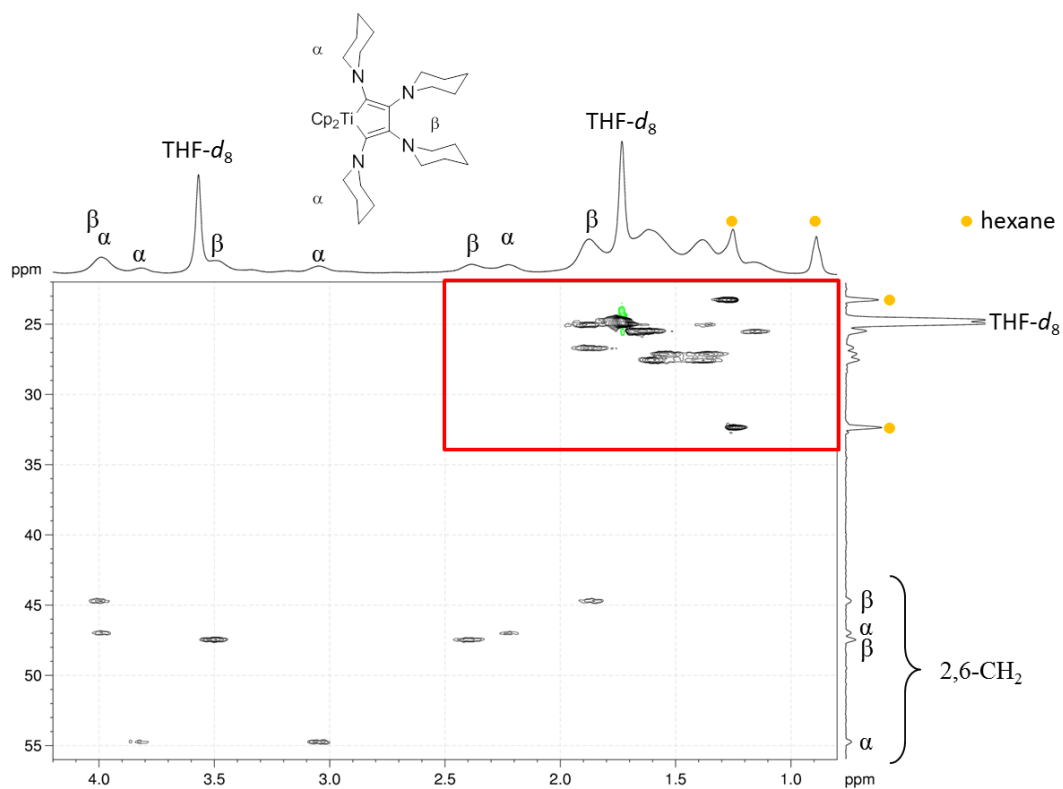
Solutions of compound **3** in THF are not stable at room temperature, and after 1 d a mixture of decomposition products is observed by NMR spectroscopy. However, the solutions are stable enough at least for 4 h at room temperature and for more than 4 d at –20 °C, which permits the NMR investigations at low temperature in THF-*d*₈.¹ Thus, ¹H NMR spectra were recorded at different temperatures. At –94 °C (179 K) 2D NMR spectra (H,H-COSY and H,C-HSQC) were recorded in order to assign the ¹H signals at this temperature.

¹H NMR spectra (298–179 K)



¹ At low temperatures, compound **3** is much more soluble in THF than in other solvents (like toluene). That is the reason why THF was preferred for this study.

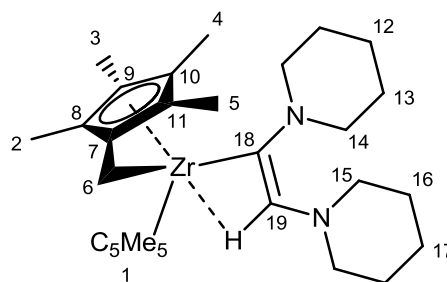
$^1\text{H}, ^{13}\text{C}$ -HSQC NMR spectrum (179 K)



2.4. NMR investigations on the pair of complexes $[\text{Cp}^*_2\text{Zr}(\text{C}_2\text{pip}_2)]$
(8a)/ $[\text{Cp}^*\text{Zr}(\text{C}_5\text{Me}_4\text{CH}_2)\{\text{C}(\text{pip})=\text{CH}(\text{pip})\}]$ (**9a**)

^1H NMR (C_6D_6 , 400.4 MHz, 297 K): Ratio **8a**:**9a** = *ca.*

1:1.3; **8a**: δ = 1.43–1.53 (m, 4H, 4- CH_2), 1.54–1.61 (br m, $\nu_{1/2} \approx 15$ Hz, 8H, 3,5- CH_2), 1.96 (s, 30H, C_5Me_5), 2.88 (t, $^3J_{2,6\text{-H},3,5\text{-H}} = 5.2$ Hz, 8H, 2,6- CH_2). **9a**: δ = 1.04 (s, 1H, 19), 1.27–1.33 (br m, $\nu_{1/2} \approx 21$ Hz, 2H, 14), 1.39 (s, 3H, 5), 1.43–1.53 (m, 6H, 13 or 16 and 17), 1.54–1.61 (br m, $\nu_{1/2} \approx 15$ Hz, 4H, 13 or 16), 1.75 (s, 3H, 2), 1.78 (s, 3H, 3), 1.92 (s, 15H, 1), 2.05 (s, 3H, 4), 2.43–2.61 (br m, $\nu_{1/2} \approx 28$ Hz, 4H, 15), 2.51 (d, $^2J_{\text{HH}} = 5.3$ Hz, 1H, 6), 2.79 (dd, $^2J_{\text{HH}} = 5.3$ Hz, $^3J_{6,19} = 0.5$ Hz, 1H, 6), 3.25–3.43 (br m, $\nu_{1/2} \approx 40$ Hz, 2H, 14), 3.54–3.73 (br m, $\nu_{1/2} \approx 42$ Hz, 2H, 14).

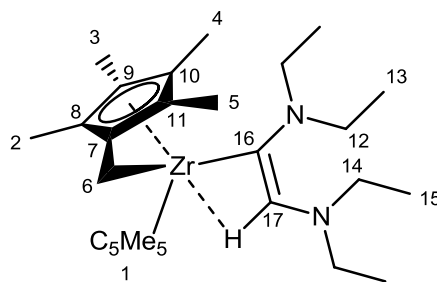


$^{13}\text{C}\{^1\text{H}\}$ NMR (C_6D_6 , 100.7 MHz, 299 K) **8a**: δ = 12.2 (C_5Me_5), 25.7 (4- CH_2), 27.4 (3,5- CH_2), 54.4 (2,6- CH_2), 119.2 (C_5Me_5), 197.8 (Zr–C(N)). **9a**: δ = 10.9 (3), 11.1 (2), 12.5 (C_5Me_5), 12.8 (4), 14.3 (5), 24.7 (12 or 17), 25.6 (12 or 17), 26.7 (16), 27.6 (13), 55.8 (6), 56.2 (15), 86.1 (19), 115.2 (C_5Me_5), 116.0 (9), 116.1 (8), 118.2 (7), 121.4 (11), 122.6 (10), 179.6 (18). The ^{13}C signal for 14 is not observed.

^{13}C NMR (toluene- d_8 , 100.7 MHz, 296 K): **8c**: δ = 12.2 (q, $^1J_{\text{C,H}} = 126$ Hz, C_5Me_5), 25.7 (t, $^1J_{\text{C,H}} = 128$ Hz, 4- CH_2), 27.4 (t, $^1J_{\text{C,H}} = 126$ Hz, 3,5- CH_2), 54.3 (t, $^1J_{\text{C,H}} = 133$ Hz, 2,6- CH_2), 119.1 (m, C_5Me_5), 197.8 (s, C_q). **8c**: δ = 10.8 (q, $^1J_{\text{C,H}} = 126$ Hz, 3), 11.1 (q, $^1J_{\text{C,H}} = 126$ Hz, 2), 12.4 (q, $^1J_{\text{C,H}} = 126$ Hz, C_5Me_5), 12.8 (q, $^1J_{\text{C,H}} = 126$ Hz, 4), 14.2 (q, $^1J_{\text{C,H}} = 126$ Hz, 5), 24.7 (t, $^1J_{\text{C,H}} = 124$ Hz, 12 or 17), 25.6 (t, $^1J_{\text{C,H}} = 123$ Hz, 12 or 17), 26.7 (t, $^1J_{\text{C,H}} = 125$ Hz, 16), 27.6 (t, $^1J_{\text{C,H}} = 127$ Hz, 13), 52.3 (t, $^1J_{\text{C,H}} = 133$ Hz, 14), 53.7 (t, $^1J_{\text{C,H}} = 133$ Hz, 14), 55.8 (t, $^1J_{\text{C,H}} = 145$ Hz, 6), 56.1 (t, $^1J_{\text{C,H}} = 133$ Hz, 15), 86.0 (d, $^1J_{\text{C,H}} = 130$ Hz, 19), 115.1 (m, C_5Me_5), 116.0 (m, 9), 116.1 (m, 8), 118.2 (m, 7), 121.3 (m, 11), 122.6 (m, 10), 179.6 (d, $^2J_{\text{C},19} = 18$ Hz, 18).

2.5. NMR investigations on the pair of complexes $[\text{Cp}^*\text{Zr}\{\text{C}_2(\text{NEt}_2)_2\}]$ (8c**)/ $[\text{Cp}^*\text{Zr}(\text{C}_5\text{Me}_4\text{CH}_2)\{\text{C}(\text{NEt}_2)=\text{CH}(\text{NEt}_2)\}]$ (**9c**)**

^1H NMR (C_6D_6 , 400.4 MHz, 297 K): Ratio **8c**:**9c** = ca. 1:2.05. **8c**: δ = 1.12 (t, $^3J_{\text{H,H}} = 7.2$ Hz, 12H, CH_3), 1.95 (s, 30H, C_5Me_5), 2.85 (q, $^3J_{\text{H,H}} = 7.2$ Hz, 8H, CH_2). **9c**: δ = 1.00 (t, $^3J_{\text{H,H}} = 7.1$ Hz, 6H, 15), 1.08–1.18 (br m, $\nu_{1/2} \approx 22$ Hz, 6H, 13), 1.18 (s, $^3J_{6,17} = 0.5$ Hz, 1H, 17), 1.37 (s, 3H, 5), 1.74 (s, 3H, 2), 1.79 (s, 3H, 3), 1.91 (s, 15H, 1), 1.97 (s, 3H, 4), 2.45 (d, $^2J_{\text{H,H}} = 5.4$ Hz, 1H, 6), 2.63, 2.65 ($2 \times$ q, $^3J_{14,15} = 7.1$ Hz, $2 \times 2\text{H}$, 14), 2.72 (dd, $^2J_{\text{H,H}} = 5.3$ Hz, $^3J_{6,17} = 0.2$ Hz, 1H, 6), 3.28–3.40 (br m, $\nu_{1/2} \approx 29$ Hz, 2H, 12), 3.50–4.10 (br m, $\nu_{1/2} \approx 120$ Hz, 2H, 12).

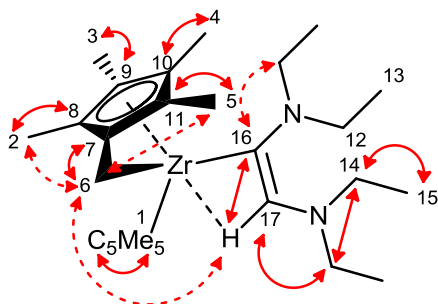


$^{13}\text{C}\{^1\text{H}\}$ NMR (C_6D_6 , 100.7 MHz, 298 K): **8c**: δ = 12.1 (C_5Me_5), 17.0 (CH_3), 51.5 (CH_2), 119.2 (C_5Me_5), 198.4 (C_q). **9c**: δ = 11.0 (3), 11.3 (2), 12.3 (15), 12.4 (C_5Me_5), 12.5 (4), 13.9 (5), 14.2–15.0 (br, 13), 40.0–41.5 (br, 12), 48.1 (14), 48.8–52.0 (br, 12), 56.2 (6), 83.0 (17), 115.3 (C_5Me_5), 116.0 (9), 116.3 (8), 118.0 (7), 121.0 (11), 122.6 (10), 179.7 (16).

^{13}C NMR (C_6D_6 , 100.7 MHz, 297 K): **8c**: δ = 12.1 (q, $^1J_{\text{C,H}} = 126$ Hz, C_5Me_5), 17.0 (q, $^1J_{\text{C,H}} = 125$ Hz, CH_3), 51.5 (tq, $^1J_{\text{C,H}} = 132$ Hz, $^3J_{\text{C,Me}} = 5$ Hz, CH_2), 119.2 (m, C_5Me_5), 198.4 (m, C_q). **9c**: δ = 11.0 (q, $^1J_{\text{C,H}} = 126$ Hz, 3), 11.3 (q, $^1J_{\text{C,H}} = 126$ Hz, 2), 12.3 (q, $^1J_{\text{C,H}} = 125$ Hz, 15), 12.4 (q, $^1J_{\text{C,H}} = 126$ Hz, C_5Me_5), 12.5 (q, $^1J_{\text{C,H}} = 126$ Hz, 4), 13.9 (q, $^1J_{\text{C,H}} = 126$ Hz, 5), 14.2–15.0 (br, 13), 40.0–41.5 (br, 12), 48.1 (t, $^1J_{\text{C,H}} = 133$ Hz, 14), 48.8–52.0 (br, 12), 56.2 (t, $^1J_{\text{C,H}} = 145$ Hz, 6), 83.0 (dp, $^1J_{\text{C,H}} = 129$ Hz, $^3J_{\text{C,14}} = 4$ Hz, 17), 115.3 (m, C_5Me_5), 116.0 (m, 9), 116.3 (m, 8), 118.0 (m, 7), 121.0 (m, 11), 122.6 (m, 10), 179.7 (d, $^2J_{\text{C,17}} = 18$ Hz, 16).

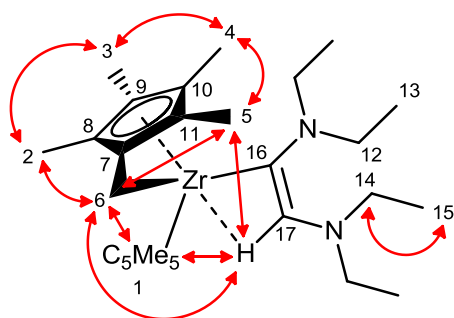
H,C-HSQC (relevant correlations, $^1\text{H} \leftrightarrow ^{13}\text{C}$): 2.45/2.72 \leftrightarrow 56.2 (6), 3.28–3.40 \leftrightarrow 40.0–41.5/48.8–52.0 (12).

H,C-HMBC: 1 (Me) \leftrightarrow 1 (C_q), 2 \leftrightarrow 6 (wk), 2 \leftrightarrow 7, 2 \leftrightarrow 8, 2 \leftrightarrow 9, 3 \leftrightarrow 6 (wk), 3 \leftrightarrow 8, 3 \leftrightarrow 9, 3 \leftrightarrow 10, 4 \leftrightarrow 6 (wk), 4 \leftrightarrow 9, 4 \leftrightarrow 10, 4 \leftrightarrow 11, 5 \leftrightarrow 6 (wk), 5 \leftrightarrow 7, 5 \leftrightarrow 10, 5 \leftrightarrow 11, 6 \leftrightarrow 7, 6 \leftrightarrow 8, 6 \leftrightarrow 11, 6 \leftrightarrow 16 (wk), 6 \leftrightarrow 17 (wk), 12 \leftrightarrow 16 (wk), 14 \leftrightarrow 14, 14 \leftrightarrow 15, 14 \leftrightarrow 17, 16 \leftrightarrow 17.



(Most relevant correlations are indicated with arrows)

H,H-NOESY: $1 \leftrightarrow 2$, $1 \leftrightarrow 3$, $1 \leftrightarrow 6$, $1 \leftrightarrow 13$, $1 \leftrightarrow 14$, $1 \leftrightarrow 15$, $1 \leftrightarrow 17$, $2 \leftrightarrow 3$, $2 \leftrightarrow 6$, $3 \leftrightarrow 4$, $4 \leftrightarrow 5$, $5 \leftrightarrow 6$, $5 \leftrightarrow 17$, $6 \leftrightarrow 6$, $6 \leftrightarrow 17$, $14 \leftrightarrow 15$. No exchange correlations were observed, although different mixing times (0.5, 1, 2 s) were tested.



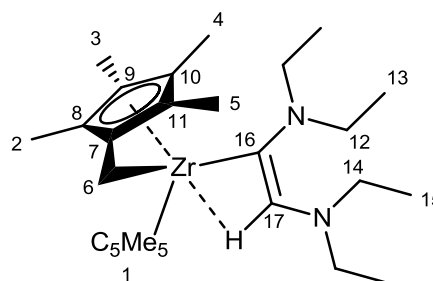
(Most relevant correlations are indicated with arrows)

High temperature NMR in toluene- d_8 (400.4 MHz, 345 K)

^1H NMR (toluene- d_8 , 400.4 MHz, 345 K): Ratio

8c:9c = ca. 1:1.2. **8c:** δ = 1.10 (t, $^3J_{\text{H,H}} = 7.2$ Hz, 12H, CH_3), 1.95 (s, 30H, C_5Me_5), 2.84 (q, $^3J_{\text{H,H}} = 7.2$ Hz, 8H, CH_2). **9c:** δ = 1.01 (t, $^3J_{\text{H,H}} = 7.1$ Hz, 6H, 15), 1.15 (t, $^3J_{\text{H,H}} = 7.1$ Hz, 6H, 13), 1.20 (s, 1H, 17), 1.32 (s, 3H, 5), 1.71 (s, 3H, 2), 1.81 (s, 3H, 3), 1.91 (s, 15H, 1), 1.97 (s, 3H, 4), 2.34 (d,

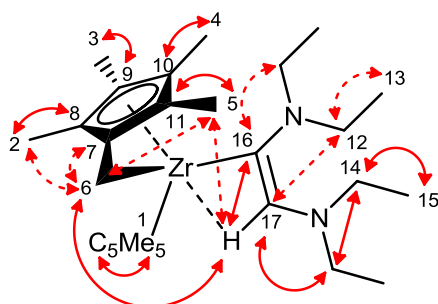
$^2J_{\text{H,H}} = 5.4$ Hz, 1H, 6), 2.61 (d, $^2J_{\text{H,H}} = 5.4$ Hz, 1H, 6), 2.63 (q, $^3J_{\text{H,H}} = 7.1$ Hz, 2H, 14), 2.64 (q, $^3J_{\text{H,H}} = 7.1$ Hz, 2H, 14), 3.37 (m, $^3J_{\text{H,H}} = 7.0$ Hz, 2H, 12), 3.55 (br m, $\nu_{1/2} \approx 27$ Hz, 2H, 12).



$^{13}\text{C}\{^1\text{H}\}$ NMR (toluene- d_8 , 101 MHz, 345 K): **8c:** δ = 12.0 (C_5Me_5), 16.7 (CH_3), 51.3 (CH_2), 119.4 (C_5Me_5), 197.8 (C_q). **9c:** δ = 10.9 (3), 11.3 (2), 12.3 (C_5Me_5), 12.4 (4), 12.6 (15), 13.9 (5), 14.7 (13), 46.0 (br, 12), 48.6 (14), 56.4 (6), 84.1 (17), 115.6 (C_5Me_5), 116.2 (9), 116.6 (8), 118.5 (7), 121.2 (11), 123.0 (10), 180.5 (16).

H,C-HSQC (relevant correlations, $^1\text{H} \leftrightarrow ^{13}\text{C}$): 2.34/2.61 \leftrightarrow 56.4 (6), 3.37/3.55 \leftrightarrow 46.0 (12).

H,C-HMBC: 1 (Me) \leftrightarrow 1 (C_q), 2 \leftrightarrow 6 (wk), 2 \leftrightarrow 7, 2 \leftrightarrow 8, 2 \leftrightarrow 9, 3 \leftrightarrow 8, 3 \leftrightarrow 9, 3 \leftrightarrow 10, 4 \leftrightarrow 9, 4 \leftrightarrow 10, 4 \leftrightarrow 11, 5 \leftrightarrow 6 (wk), 5 \leftrightarrow 7, 5 \leftrightarrow 10, 5 \leftrightarrow 11, 5 \leftrightarrow 17 (wk), 6 \leftrightarrow 7 (wk), 6 \leftrightarrow 8, 6 \leftrightarrow 11, 6 \leftrightarrow 16 (wk), 6 \leftrightarrow 17, 12 \leftrightarrow 13 (wk), 12 \leftrightarrow 16 (wk), 12 \leftrightarrow 17 (wk), 14 \leftrightarrow 14, 14 \leftrightarrow 15, 14 \leftrightarrow 17, 16 \leftrightarrow 17.

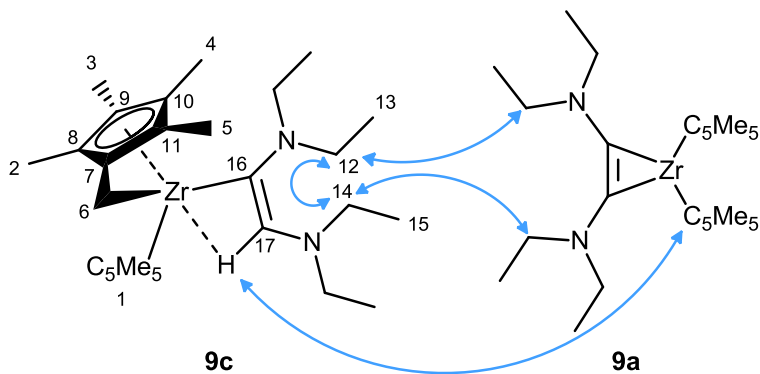


(Most relevant correlations are indicated with arrows)

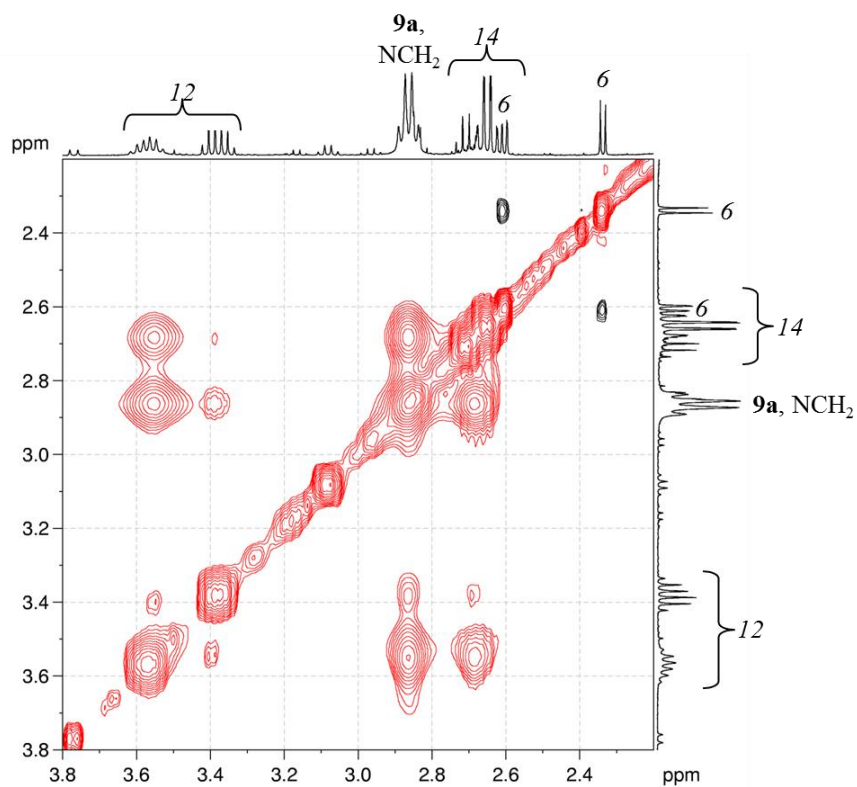
High temperature NMR in toluene- d_8 (400.4 MHz, 376 K)

H,H-COSY: $6 \leftrightarrow 6$, $12 \leftrightarrow 12$, $12 \leftrightarrow 13$, $14 \leftrightarrow 15$.

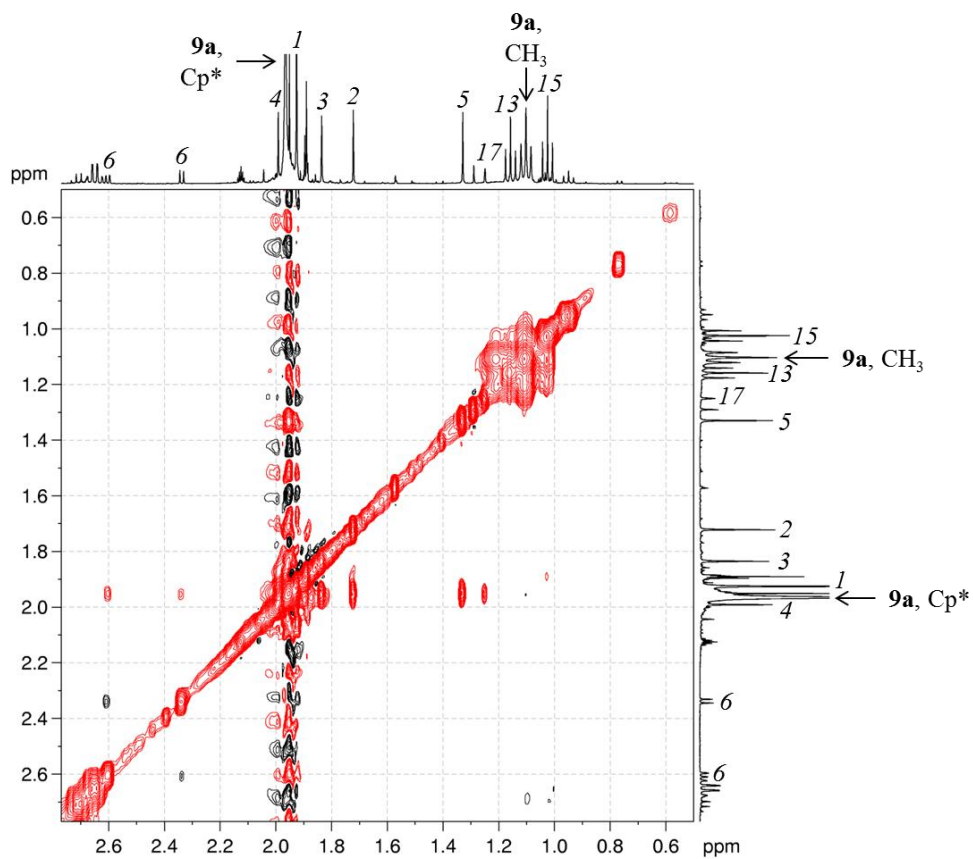
H,H-EXSY (H,H-NOESY, mixing time 1 s): $2 \leftrightarrow C_5Me_5$, $3 \leftrightarrow C_5Me_5$, $5 \leftrightarrow C_5Me_5$, $12 \leftrightarrow 14$, $12 \leftrightarrow CH_2$, $14 \leftrightarrow CH_2$, $17 \leftrightarrow C_5Me_5$.



(Most relevant exchange-correlations are indicated with blue arrows)

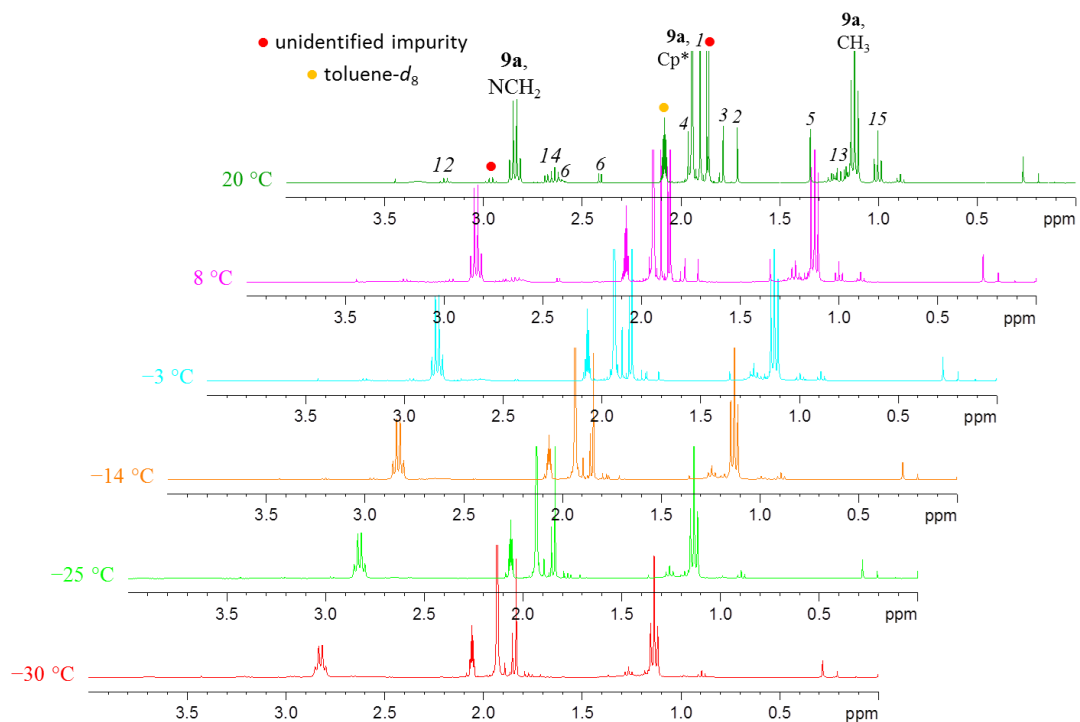


(exchange-peaks are depicted in red, whereas cross-peaks are depicted in black)



(exchange-peaks are depicted in red, whereas cross-peaks are depicted in black)

Low temperature NMR (243–293 K)

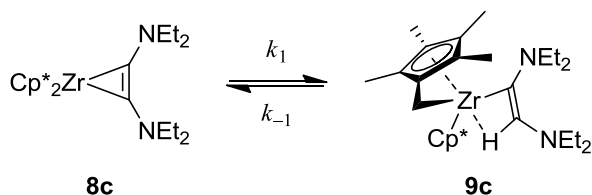


3. Kinetic study

A sample of crystalline, pure $[\text{Cp}^*_2\text{Zr}\{\text{C}_2(\text{NEt}_2)_2\}]$ (**8c**) was dissolved in toluene- d_8 at $-35\text{ }^\circ\text{C}$ in an NMR tube. The NMR tube was placed in a previously cooled spectrometer at $-30\text{ }^\circ\text{C}$, and the temperature was increased stepwise. For each temperature, two ^1H NMR spectra were recorded over an interval of 30 min. It was observed that **8c** was slowly converted into **9c**, caused both by the temperature increments and the time lapses. The ratio **8c:9c** (equal to the equilibrium constant K) was determined by integration of the Cp* signals of both compounds (30H:15H, resp.). At $20\text{ }^\circ\text{C}$ the conversion was fast enough to follow it over a reasonable period of time, so that ^1H NMR spectra were recorded every 15 min until the equilibrium was reached. The results are arranged in Table S1.

Table S1. Ratio **8c:9c** as a Function of Time at Different Temperatures

$T/^\circ\text{C}$	T/K	entry	$t/\text{h}:\text{min}$	t/s	χ_{8c}	χ_{9c}	8c:9c = K
-30	243	1	0:00	0	0.972	0.028	0.029
		2	0:37	2220	0.968	0.032	0.033
-25	248	3	0:48	2880	0.965	0.035	0.036
		4	1:17	4620	0.957	0.043	0.045
-14	259	5	1:32	5520	0.951	0.049	0.052
		6	2:02	7320	0.938	0.062	0.066
-3	270	7	2:14	8040	0.935	0.065	0.070
		8	2:48	10080	0.899	0.101	0.113
8	281	9	3:01	10860	0.867	0.133	0.153
		10	3:33	12780	0.769	0.231	0.300
20	293	11	3:48	13680	0.684	0.316	0.463
		12	4:03	14580	0.605	0.395	0.653
		13	4:18	15480	0.526	0.474	0.901
		14	4:33	16380	0.476	0.524	1.100
		15	4:48	17280	0.439	0.561	1.278
		16	5:03	18180	0.411	0.589	1.431
		17	5:18	19080	0.389	0.611	1.569
		18	5:33	19980	0.373	0.627	1.683
		19	5:48	20880	0.358	0.642	1.793
		20	6:21	22860	0.340	0.660	1.937
		21	6:43	24180	0.335	0.665	1.983
		22	7:04	25440	0.327	0.673	2.057
		23	7:26	26760	0.330	0.670	2.032
		24	7:47	28020	0.324	0.676	2.086
		25	8:08	29280	0.329	0.671	2.037
		26	8:30	30600	0.327	0.673	2.054
		27	8:51	31860	0.330	0.670	2.032



Scheme S1. Equilibrium reaction of **8c** and **9c**, showing the corresponding rate constants for the conversion of **8c** into **9c** (k_1) and vice versa (k_{-1}).

The first nine recordings at 20 °C (entries 11–19) were taken in consideration in order to determine the rate constant of the conversion (Scheme 1), and that is why the time was set again to zero from entry 11 on (see Table 2).² Thus, the conversion was treated as a first-order reaction proceeding to equilibrium, which can be expressed by the following rate equation (see the Appendix for details):³

$$-d(A_{8c,t})/dt = d(A_{9c,t})/dt = k_1 \cdot A_{8c,t} - k_{-1} \cdot A_{9c,t}$$

where $A_{8c,t}$ and $A_{9c,t}$ represent the relative integrals of the ¹H NMR Cp* signals at the time of the measurement (t) for complexes **8c** and **9c**, respectively, and k_1 and k_{-1} are the equilibrium rate constants (see Scheme S1). Considering that $A_{8c,t} + A_{9c,t} = 1$ applies, the terms can be rearranged and the resulting equation can be integrated between $t = 0$ and t , and $A_{9c,t} = A_{9c,0}$ and $A_{9c,t}$, giving the following linear equation:

$$-\ln(A_{9c,\infty} - A_{9c,t}) = k_{\text{obs}}t - \ln(A_{9c,0} - A_{9c,\infty})$$

where $k_{\text{obs}} = k_1 + k_{-1}$, and $A_{9c,0}$ and $A_{9c,\infty}$ represent the relative integrals of the ¹H NMR Cp* signals for complex **9c** at $t = 0$ and at equilibrium, respectively. The latter was given a value of 0.67, which results from the arithmetical mean of the $A_{9c,t}$ values at equilibrium (Table S1, entries 22–27).

The normal logarithms of the difference of the relative integrals of **9c** at equilibrium and at the time of the measurement (Table S2) were plotted against the time of the measurement (t), affording a linear arrangement from which a linear regression was applied (Figure S1). The following equation is obtained:

$$-\ln(A_{9c,\infty} - A_{9c,t}) = 3.38 \cdot 10^{-4}t - 1.00$$

with a correlation coefficient of $r = 0.9991$ and standard errors of $0.05 \cdot 10^{-4}$ and 0.02 for the slope and for the intersection, respectively.

² That does not affect the slope of the regression line (k_{obs}), only the intersection, which is not relevant for the subsequent calculations.

Table S2. Excerpt of Table S1 with the Selected Entries for the Plotting, Showing the Corresponding Time Adjustments and Calculated Logarithms

T/K	entry	t/s	t(20 °C)/s	$A_{8c,t}$	$A_{9c,t}$	$-\ln(A_{9c,\infty}-A_{9c,t})$
293	11	13680	0	0.684	0.316	1.034
	12	14580	900	0.605	0.395	1.283
	13	15480	1800	0.526	0.474	1.619
	14	16380	2700	0.476	0.524	1.909
	15	17280	3600	0.439	0.561	2.197
	16	18180	4500	0.411	0.589	2.484
	17	19080	5400	0.389	0.611	2.790
	18	19980	6300	0.373	0.627	3.106
	19	20880	7200	0.358	0.642	3.500

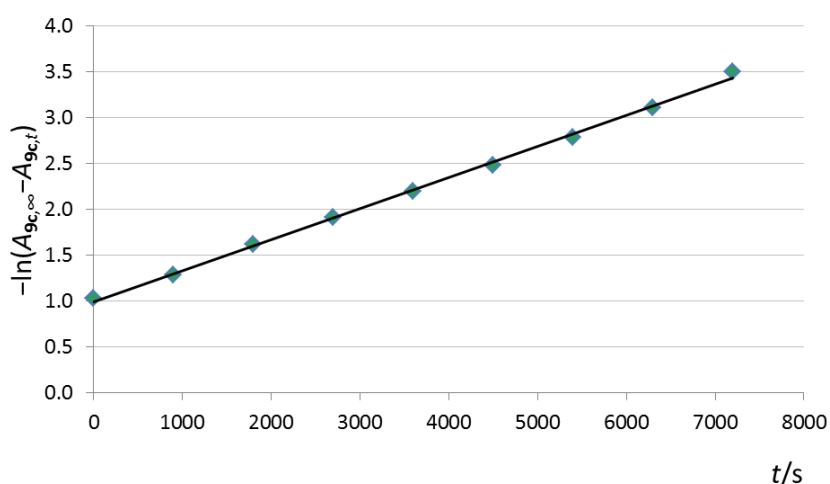


Figure S1. First-order kinetic plot for the conversion of **8c** to **9c** at 293 K, showing the linear relationship of the logarithms of the relative integral differences against the time of the measurement.

The slope of the obtained linear equation is directly k_{obs} , which is the sum of the rate constants k_1 and k_{-1} . These can be determined using the relationship of the equilibrium constant (K) with them:

$$K = A_{9c,\infty}/A_{8c,\infty} = k_1/k_{-1}$$

Given $\bar{A}_{9c,\infty} = 0.67(1)$ and $\bar{A}_{8c,\infty} = 0.33(1)$ (the arithmetical mean of the relative integrals of **9c** and **8c** at equilibrium, $A_{9c,\infty}$ and $A_{8c,\infty}$, respectively (Table S1, entries 22–27)), the constants $k_1 = 2.27(7) \cdot 10^{-4} \text{ s}^{-1}$ and $k_{-1} = 1.11(5) \cdot 10^{-4} \text{ s}^{-1}$ are obtained (see the Appendix for details).

In addition, the half-life times ($t_{1/2(1)}$ and $t_{1/2(-)}$) can be estimated as follows:

$$t_{1/2(1)} = \ln(2) (k_1)^{-1} = 3051 \text{ s} = 50.9(15) \text{ min}$$

$$t_{1/2(-1)} = \ln(2) (k_{-1})^{-1} = 6254 \text{ s} = 104(5) \text{ min}$$

Finally, the Gibbs energy differences for the transition state of complexes **8c** and **9c** (ΔG_1^\ddagger and ΔG_{-1}^\ddagger , respectively) at 293 K can be determined using the Eyring equation:

$$k = \frac{k_B T}{h} e^{-\frac{\Delta G^\ddagger}{RT}} \Rightarrow \Delta G^\ddagger = -RT \ln \left(\frac{hk}{k_B T} \right)$$

where k is the rate constant, T is the temperature (293 K), k_B is the Boltzmann constant, h is the Planck constant, and R is the universal gas constant. For k_1 and k_{-1} the following values are obtained:

$$\Delta G_1^\ddagger = 9.22(7) \cdot 10^{-4} \text{ J mol}^{-1} = 22.0(2) \text{ kcal mol}^{-1}$$

$$\Delta G_{-1}^\ddagger = 9.40(8) \cdot 10^{-4} \text{ J mol}^{-1} = 22.5(2) \text{ kcal mol}^{-1}$$

4. Crystallographic data

Table S3. Crystallographic Data for Complexes **3**, **5**, **7**, **8a**, [**8a**·MgCl₂]₂, **8b** and **8c**.

	3 ·½(<i>n</i> -C ₆ H ₁₄)	5 ·½C ₆ H ₆	7	8a	[8a ·MgCl ₂] ₂ · <i>n</i> -C ₆ H ₁₄	8b	8c
empirical formula	C ₃₇ H ₅₇ N ₄ Ti	C ₃₇ H ₅₃ N ₄ Zr	C ₃₂ H ₅₀ N ₂ Ti	C ₃₂ H ₅₀ N ₂ Zr	C ₇₀ H ₁₁₄ Cl ₄ Mg ₂ N ₄ Zr ₂	C ₃₄ H ₅₄ N ₂ Zr	C ₃₀ H ₅₀ N ₂ Zr
<i>M_w</i>	605.77	645.05	510.64	553.96	1382.50	582.01	529.94
wavelength (Å)	0.71073	1.54184	0.71073	0.71073	1.54184	0.71073	1.54184
<i>T</i> (K)	100(2)	100(2)	100(2)	150(2)	100(2)	100(2)	100(2)
cryst size (mm)	0.18 × 0.16 × 0.10	0.05 × 0.02 × 0.01	0.38 × 0.27 × 0.20	0.35 × 0.21 × 0.16	0.17 × 0.11 × 0.03	0.3 × 0.2 × 0.1	0.20 × 0.10 × 0.05
cryst system	monoclinic	orthorhombic	monoclinic	monoclinic	monoclinic	monoclinic	triclinic
space group	<i>C2/c</i>	<i>Pbca</i>	<i>P2₁/n</i>	<i>P2₁/n</i>	<i>P2₁/n</i>	<i>C2/c</i>	<i>P</i> $\bar{1}$
<i>a</i> (Å)	42.983(2)	8.1846(7)	9.5997	9.7554(2)	9.3404(2)	21.5996(9)	10.2288(7)
<i>b</i> (Å)	10.0244(4)	20.3198(16)	29.1028(4)	29.1238(5)	30.3129(4)	11.7559(3)	11.7739(7)
<i>c</i> (Å)	15.7383(8)	39.301(4)	10.6135(2)	10.8155(2)	12.4741(2)	14.5295(6)	14.2956(8)
α (°)	90	90	90	90	90	90	90.487(5)
β (°)	102.501(4)	90	102.455(2)	103.129(1)	93.136(2)	121.651(6)	110.835(6)
γ (°)	90	90	90	90	90	90	114.542(6)
<i>V</i> (Å ³)	6620.5(5)	6536.1(9)	2895.40(9)	2992.52(10)	3526.56(11)	3140.6(2)	1438.78(15)
<i>Z</i>	8	8	4	4	2	4	2
ρ_{calc} (Mg m ⁻³)	1.215	1.311	1.171	1.230	1.302	1.231	1.223
μ (mm ⁻¹)	0.290	2.981	0.318	0.389	4.301	0.374	3.249
<i>F</i> (000)	2632	2744	1112	1184	1464	1248	568
reflx collected	108490	135134	139622	66816	57547	73753	45336
indep reflx (<i>R</i> _{int})	6774 (0.0801)	5774 (0.2653)	6905 (0.0297)	6864 (0.0344)	7209 (0.0336)	4793 (0.0451)	5952 (0.0613)
GoF on <i>F</i> ²	1.114	1.133	1.131	1.087	1.053	1.057	1.026
<i>R</i> ₁ (<i>I</i> > 2σ(<i>I</i>))	0.0475	0.0647	0.0353	0.0262	0.0249	0.0275	0.0218
w <i>R</i> ₂ (all refl.)	0.1019	0.1245	0.0858	0.0641	0.0627	0.0685	0.0549

5. Computational details

5.1. Optimized structures

The structures of the complexes' pairs **8a/9a** and **8c/9c** were investigated by density functional theory (DFT) computations applying the functionals B97-D/6-311g(d,p)⁴ and M06-2X/6-311g(d,p)⁵ as implemented in the Gaussian09 program.⁶ For both pairs also a transition state (**TS(a)** and **TS(c)**, respectively) was calculated. Selected structural parameters of all the optimized structures are collected in tables S4 and S5 and compared with the XRD data of the zirconacycloprenes **8a** and **8c**, respectively. The optimized structures with the corresponding numbering are depicted in figs. S2–5.

Table S4. Selected Bond Distances [Å] and Angles [°] for the Calculated Structures (B97-D and M06-2X Functionals) of Complexes **8a** and **9a**, and of a Possible Transition State **TS(a)**, Compared with the Structural Parameters for Complex **8a** Determined by XRD Analysis

	8a			TS(a)		9a	
	XRD	B97-D	M06-2X	B97-D	M06-2X	B97-D	M06-2X
C1–C2	1.344(2)	1.352	1.343	1.342	1.332	1.359	1.349
Zr–C1	2.1545(13)	2.160	2.160	2.278	2.286	2.702	2.714
Zr–C2	2.1566(14)	2.160	2.162	2.185	2.190	2.275	2.283
C1–N1	1.4025(19)	1.391	1.395	1.413	1.418	1.439	1.438
C2–N2	1.4042(19)	1.393	1.397	1.380	1.382	1.375	1.378
C3–C4	1.502(2)	1.504	1.501	1.484	1.483	1.457	1.458
Zr–C3	–	–	–	2.468	2.466	2.392	2.369
Zr–C4	2.5358(16)	2.550	2.562	2.342	2.332	2.296	2.287
Zr–H1	–	–	–	1.913	1.935	2.366	2.385
C3–H1	0.9811(18)	–	–	1.503	1.499	2.979	2.943
C1–H1	–	–	–	1.626	1.618	1.118	1.114
Zr–Ct1 ^a	2.2642(1)	2.291	2.289	2.268	2.246	2.214	2.199
Zr–Ct2 ^a	2.2667(1)	2.291	2.292	2.284	2.290	2.290	2.291
Ct1–C4–C3	174.43(14)	175.31	174.97	147.98	147.62	145.95	145.00
Ct1–Zr–Ct2 ^a	137.368(7)	138.43	137.03	138.22	138.05	139.68	138.77
Ct1–Zr–Ct _{C1C2} ^a	111.138(6)	110.87	111.48	109.25	108.90	112.07	111.85
Ct2–Zr–Ct _{C1C2} ^a	111.490(6)	110.69	111.49	111.07	111.75	106.43	107.59
C1–Zr–C2	36.32(5)	36.47	36.21	34.91	34.54	30.17	29.77
C2–C1–Zr	71.75(9)	71.79	71.79	76.31	76.71	92.58	93.10
C1–C2–Zr	71.92(9)	71.74	72.00	68.78	68.76	57.26	57.13
N1–C1–C2	130.88(14)	132.53	131.67	132.29	132.11	128.92	128.31
C1–C2–N2	130.95(14)	132.74	132.03	130.83	130.32	131.90	131.91
N1–C1–C2–N2	0.6(3)	2.6	2.7	–5.6	–5.0	–1.8	–5.1
ϕ^b	40.29(6)	39.2	41.0	39.7	40.0	39.7	40.2

^a Ct1, Ct2 = centroid of the Cp rings; Ct_{C1C2} = center of the C1–C2 bond.

^b Dihedral angle between the least-squares planes of the Cp rings.

Table S5. Selected Bond Distances [Å] and Angles [°] for the Calculated Structures (B97-D and M06-2X Functionals) of Complexes **8c** and **9c**, and of a Possible Transition State **TS(c)**, Compared with the Structural Parameters for Complex **8c** Determined by XRD Analysis

	8c			TS(c)		9c	
	XRD	B97-D	M06-2X	B97-D	M06-2X	B97-D	M06-2X
C1–C2	1.345(2)	1.354	1.345	1.344	1.333	1.356	1.349
Zr–C1	2.1709(14)	2.154	2.156	2.270	2.273	2.628	2.655
Zr–C2	2.1663(13)	2.154	2.156	2.186	2.189	2.268	2.282
C1–N1	1.4060(19)	1.395	1.395	1.409	1.412	1.442	1.442
C2–N2	1.4090(17)	1.395	1.395	1.389	1.391	1.360	1.363
C3–C4	1.501(3)	1.504	1.501	1.484	1.484	1.456	1.455
Zr–C3	–	–	–	2.471	2.471	2.409	2.392
Zr–C4	2.5431(17)	2.559	2.565	2.343	2.335	2.305	2.294
Zr–H1	–	–	–	1.907	1.928	2.210	2.250
C3–H1	0.9803(16)	–	–	1.495	1.488	2.728	2.710
C1–H1	–	–	–	1.596	1.592	1.131	1.125
Zr–Ct1 ^a	2.2642(2)	2.295	2.293	2.281	2.250	2.221	2.201
Zr–Ct2 ^a	2.2602(2)	2.295	2.293	2.282	2.290	2.277	2.287
Ct1–C4–C3 ^a	174.36(17)	175.48	174.74	148.65	147.84	146.39	145.61
Ct1–Zr–Ct2 ^a	137.160(6)	138.13	136.75	138.38	138.50	138.51	137.88
Ct1–Zr–Ct _{C1C2} ^a	111.511(6)	110.92	111.64	110.35	109.41	111.78	111.75
Ct2–Zr–Ct _{C1C2} ^a	111.326(7)	110.95	111.61	110.07	111.03	107.30	107.82
C1–Zr–C2	36.14(5)	36.66	36.34	35.04	34.72	31.08	30.54
C2–C1–Zr	71.74(9)	71.67	71.83	69.05	69.20	59.65	59.25
C1–C2–Zr	72.12(8)	71.68	71.82	75.91	76.09	89.28	90.21
N1–C1–C2	131.58(13)	132.94	132.55	133.12	132.50	133.49	133.69
C1–C2–N2	131.77(13)	132.96	132.55	133.20	132.47	130.05	129.24
N1–C1–C2–N2	5.0(3)	7.6	7.4	–8.1	–8.0	–0.8	–3.8
ϕ^b	41.30(6)	40.3	42.4	39.5	40.2	40.1	40.4

^a Ct1, Ct2 = centroid of the Cp rings; Ct_{C1C2} = center of the C1-C2 bond.

^b Dihedral angle between the least-squares planes of the Cp rings.

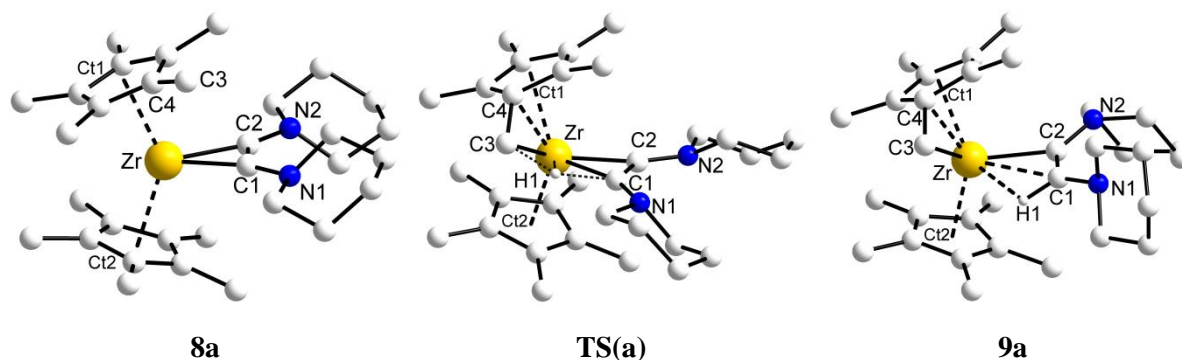


Figure S2. DIAMOND⁷ plots of the optimized structures of complexes **8a** and **9a**, and of the proposed transition state **TS(a)**, calculated with the B97-D functional.

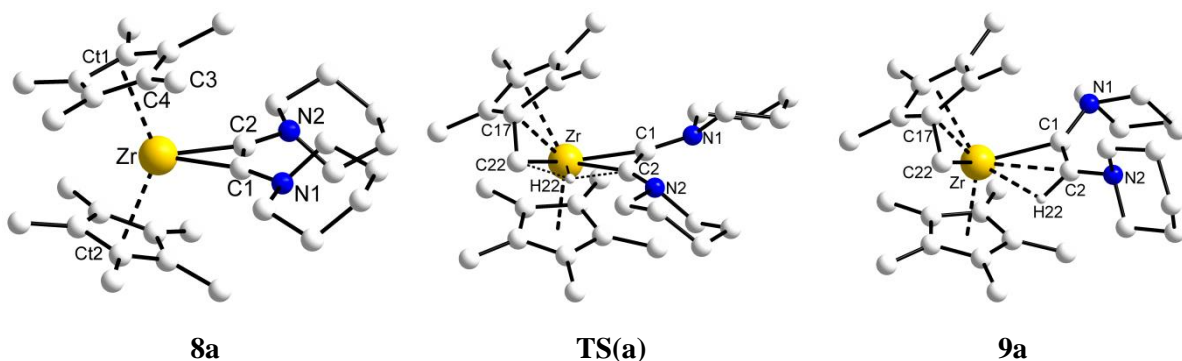


Figure S3. DIAMOND⁷ plots of the optimized structures of complexes **8a** and **9a**, and of the proposed transition state **TS(a)**, calculated with the M06-2X functional.

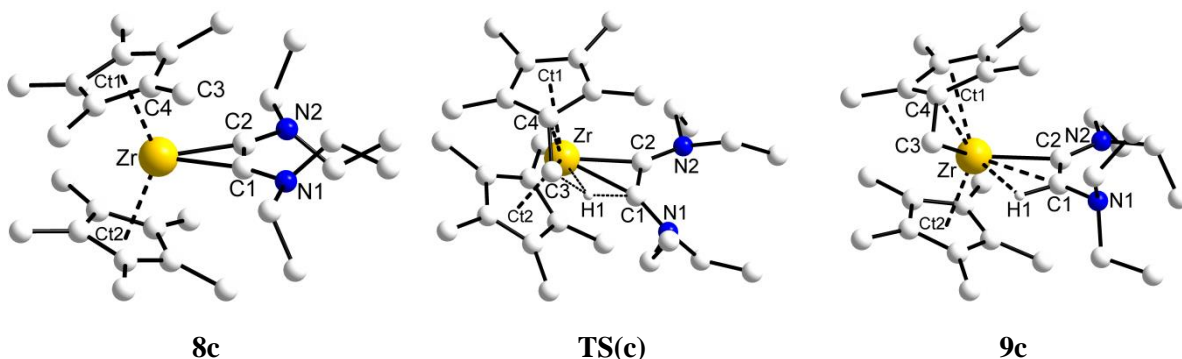


Figure S4. DIAMOND⁷ plots of the optimized structures of complexes **8c** and **9c**, and of the proposed transition state **TS(c)**, calculated with the B97-D functional.

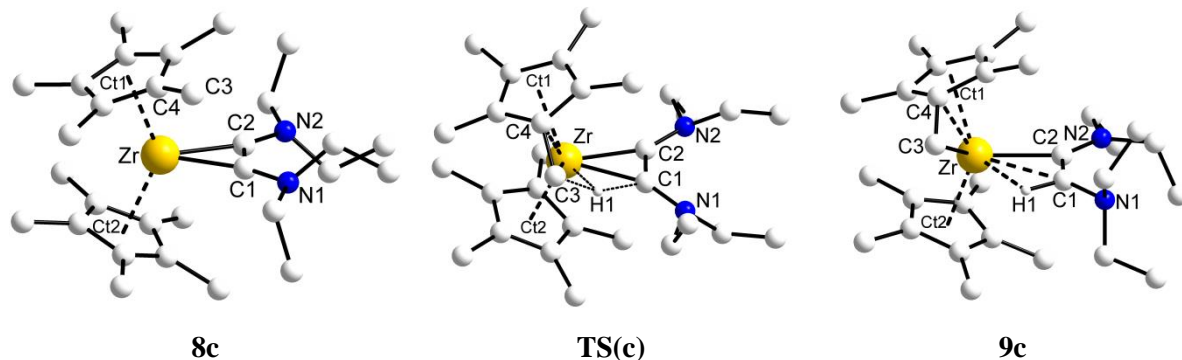


Figure S5. DIAMOND⁷ plots of the optimized structures of complexes **8c** and **9c**, and of the proposed transition state **TS(c)**, calculated with the M06-2X functional.

5.2. Thermodynamic parameters

For all structures (**8a**, **9a**, **TS(a)**, **8c**, **9c**, **TS(c)**) and methods (B97-D, M06-2X) full thermodynamic data were estimated, including the relative DFT energies including the zero-point energy (E_0), the relative DFT energies at 298 K (E_{298}), the relative enthalpies at 298 K (H_{298}), the relative Gibbs free energies at 298 K (G_{298}), and the relative electronic energies (E_{El}); the calculated values are assembled in Table S6. In addition, the energy differences in kcal mol⁻¹ for all cases are arranged in Table S7.

Table S6. Calculated Thermodynamic Parameters for Complexes **8a**, **8c**, **9a**, and **9c**, and for the Corresponding Transition States **TS(a)** and **TS(c)**

	Method	8a	TS(a)	9a	8c	TS(c)	9c
E_0/Ha	B97-D	-1404.8948	-1404.8564	-1404.8906	-1328.7348	-1328.6979	-1328.7314
	M06-2X	-1405.0250	-1404.9817	-1405.0223	-1328.8207	-1328.7766	-1328.8162
E_{298}/Ha^a	B97-D	-1404.8527	-1404.8164	-1404.8504	-1328.6915	-1328.6559	-1328.6892
	M06-2X	-1404.9847	-1404.9428	-1404.9835	-1328.7786	-1328.7359	-1328.7752
H_{298}/Ha^a	B97-D	-1404.8517	-1404.8155	-1404.8494	-1328.6905	-1328.6550	-1328.6883
	M06-2X	-1404.9837	-1404.9419	-1404.9826	-1328.7777	-1328.7350	-1328.7743
G_{298}/Ha^a	B97-D	-1404.9682	-1404.9251	-1404.9594	-1328.8097	-1328.7679	-1328.8024
	M06-2X	-1405.0957	-1405.0491	-1405.0888	-1328.8915	-1328.8445	-1328.8853
E_{El}/Ha	B97-D	-1405.6257	-1405.5863	-1405.6240	-1329.4495	-1329.4100	-1329.4472
	M06-2X	-1405.7831	-1405.7363	-1405.7818	-1329.5602	-1329.5125	-1329.5572

^a standard conditions $T = 298.15$ K and $p = 1$ atm.

Table S7. Energy Differences in kcal mol⁻¹ for the Estimated Values Displayed in Table 5

	Method	9a-8a	TS(a)-8a	TS(a)-9a	9c-8c	TS(c)-8c	TS(c)-9c
$\Delta E_0/\text{kcal mol}^{-1}$	B97-D	2.6	24.1	21.5	2.1	23.2	21.0
	M06-2X	1.7	27.1	25.4	2.8	27.6	24.9
$\Delta E_{298}/\text{kcal mol}^{-1 a}$	B97-D	1.4	22.7	21.3	1.4	22.3	20.9
	M06-2X	0.7	26.3	25.5	2.1	26.8	24.6
$\Delta H_{298}/\text{kcal mol}^{-1 a}$	B97-D	1.4	22.7	21.3	1.4	22.3	20.9
	M06-2X	0.7	26.3	25.5	2.1	26.8	24.6
$\Delta G_{298}/\text{kcal mol}^{-1 a}$	B97-D	5.5	27.0	21.5	4.6	26.2	21.6
	M06-2X	4.3	29.2	24.9	3.9	29.4	25.6
$\Delta E_{El}/\text{kcal mol}^{-1}$	B97-D	1.1	24.7	23.7	1.4	24.8	23.4
	M06-2X	0.8	29.3	28.5	1.9	29.9	28.0

^a standard conditions $T = 298.15$ K and $p = 1$ atm.

6. References

- (1) Burlakov, V. V.; Polyakov, A. V.; Yanovsky, A. I.; Struchkov, Y. T.; Shur, V. B.; Vol'pin, M. E.; Rosenthal, U.; Görls, H. *J. Organomet. Chem.* **1994**, *476*, 197–206.
- (2) Hiller, J.; Thewalt, U.; Polášek, M.; Petrusová, L.; Varga, V.; Sedmera, P.; Mach, K. *Organometallics* **1996**, *15*, 3752–3759.
- (3) Chipperfield, R. J. *J. Organomet. Chem.* **1989**, *363*, 253–263.
- (4) Grimme, S. *J. Comput. Chem.* **2006**, *27*, 1787–1799.
- (5) Zhao, Y.; Truhlar, D. G. *Acc. Chem. Res.* **2008**, *41*, 157–167.
- (6) Frisch, M. J.; Trucks, G. W.; Schlegel, H. B.; Scuseria, G. E.; Robb, M. A.; Cheeseman, J. R.; Scalmani, G.; Barone, V.; Mennucci, B.; Petersson, G. A.; Nakatsuji, H.; Caricato, M.; Li, X.; Hratchian, H. P.; Izmaylov, A. F.; Bloino, J.; Zheng, G.; Sonnenberg, J. L.; Hada, M.; Ehara, M.; Toyota, K.; Fukuda, R.; Hasegawa, J.; Ishida, M.; Nakajima, T.; Honda, Y.; Kitao, O.; Nakai, H.; Vreven, T.; Jr., J. A. M.; Peralta, J. E.; Ogliaro, F.; Bearpark, M.; Heyd, J. J.; Brothers, E.; Kudin, K. N.; Staroverov, V. N.; Kobayashi, R.; Normand, J.; Raghavachari, K.; Rendell, A.; Burant, J. C.; Iyengar, S. S.; Tomasi, J.; Cossi, M.; Rega, N.; Millam, J. M.; Klene, M.; Knox, J. E.; Cross, J. B.; Bakken, V.; Adamo, C.; Jaramillo, J.; Gomperts, R.; Stratmann, R. E.; Yazyev, O.; Austin, A. J.; Cammi, R.; Pomelli, C.; Ochterski, J. W.; Martin, R. L.; Morokuma, K.; Zakrzewski, V. G.; Voth, G. A.; Salvador, P.; Dannenberg, J. J.; Dapprich, S.; Daniels, A. D.; Farkas, Ö.; Foresman, J. B.; Ortiz, J. V.; Cioslowski, J.; Fox, D. J. *Gaussian 09*, Revision A.1; Gaussian, Inc.: Wallingford, CT (U.S.A.), 2009.
- (7) Brandenburg, K. *DIAMOND*, Version 3.1f; Crystal Impact GbR: Bonn (Germany), 2008.

7. Appendix

7.1. Deduction of the linearized rate equation

In the following deduction, $A_{8c,t} + A_{9c,t} = 1$ applies (also for $t = 0$ and $t = \infty$).

From the general rate law the following rate equation can be written:

$$\frac{-dA_{8c,t}}{dt} = \frac{dA_{9c,t}}{dt} = k_1 A_{8c,t} - k_{-1} A_{9c,t}$$

that can be rearranged as follows:

$$\begin{aligned} k_1 A_{8c,t} - k_{-1} A_{9c,t} &= k_1 (1 - A_{9c,t}) - k_{-1} A_{9c,t} = k_1 - k_1 A_{9c,t} - k_{-1} A_{9c,t} = k_1 - \\ A_{9c,t} (k_1 + k_{-1}) &= k_1 - k_{obs} A_{9c,t} = k_{-1} \frac{A_{9c,\infty}}{A_{8c,\infty}} - k_{obs} A_{9c,t} = k_{obs} A_{9c,\infty} - k_{obs} A_{9c,t} = \\ k_{obs} (A_{9c,\infty} - A_{9c,t}) \end{aligned}$$

since: $k_1 A_{8c,\infty} = k_{-1} A_{9c,\infty}$

$$\text{and: } k_{obs} = k_1 + k_{-1} = k_{-1} \frac{A_{9c,\infty}}{A_{8c,\infty}} + k_{-1} = k_{-1} \left(\frac{A_{9c,\infty}}{A_{8c,\infty}} + 1 \right) = k_{-1} \left(\frac{A_{9c,\infty} + A_{8c,\infty}}{A_{8c,\infty}} \right) = \frac{k_{-1}}{A_{8c,\infty}}$$

Integration of $\frac{dA_{9c,t}}{dt} = k_{obs} (A_{9c,\infty} - A_{9c,t})$ between $t = 0$ and t , and $A_{9c,t} = A_{9c,0}$ and $A_{9c,t}$,

$$\int_{A_{9c,0}}^{A_{9c,t}} \frac{dA_{9c,t}}{A_{9c,\infty} - A_{9c,t}} = k_{obs} \int_0^t dt, \text{ gives: } -\ln(A_{9c,\infty} - A_{9c,t}) + \ln(A_{9c,\infty} - A_{9c,0}) = k_{obs} t$$

that can be rearranged in the form of a linear equation ($y = ax + b$):

$$\ln(A_{9c,\infty} - A_{9c,t}) = -k_{obs} t + \ln(A_{9c,\infty} - A_{9c,0})$$

7.2. Deduction of the rate constants k_1 and k_{-1}

The rate constants can be calculated from the reaction constant k_{obs} as follows.

$$\text{Since: } K = \frac{A_{9c,\infty}}{A_{8c,\infty}} = \frac{k_1}{k_{-1}}, \text{ or rearranged: } k_1 A_{8c,\infty} = k_{-1} A_{9c,\infty}$$

$$\text{then: } k_{obs} = k_1 + k_{-1} = k_{-1} \frac{A_{9c,\infty}}{A_{8c,\infty}} + k_{-1} = k_{-1} \left(\frac{A_{9c,\infty}}{A_{8c,\infty}} + 1 \right) = k_{-1} \left(\frac{A_{9c,\infty} + A_{8c,\infty}}{A_{8c,\infty}} \right) = \frac{k_{-1}}{A_{8c,\infty}}$$

$$\text{and: } k_{obs} = k_1 + k_{-1} = k_{-1} + k_1 \frac{A_{8c,\infty}}{A_{9c,\infty}} = k_1 \left(\frac{A_{8c,\infty} + A_{9c,\infty}}{A_{9c,\infty}} \right) = \frac{k_1}{A_{9c,\infty}}$$

In consequence, $k_1 = k_{obs} A_{9c,\infty}$ and $k_{-1} = k_{obs} A_{8c,\infty}$